

Mechanism analysis of regulating Turing instability and Hopf bifurcation of malware propagation in mobile wireless sensor networks

Xi-Xi Huang(黄习习), Min Xiao(肖敏), Leszek Rutkowski, Hai-Bo Bao(包海波), Xia Huang(黄霞), and Jin-De Cao(曹进德)

Citation: Chin. Phys. B, 2024, 33 (**6**): 060202. DOI: 10.1088/1674-1056/ad24d5
Journal homepage: http://cpb.iphy.ac.cn; http://iopscience.iop.org/cpb

What follows is a list of articles you may be interested in

Observer-based dynamic event-triggered control for distributed parameter systems over mobile sensor-plus-actuator networks

Wenying Mu(穆文英), Bo Zhuang(庄波), and Fang Qiu(邱芳)
Chin. Phys. B, 2024, 33 (**4**): 040204. DOI: 10.1088/1674-1056/ad1a8c

Thermal-contact capacity of one-dimensional attractive Gaudin—Yang model

Xiao-Min Zhang(张小敏), Song Cheng(程颂), and Yang-Yang Chen(陈洋洋)
Chin. Phys. B, 2024, 33 (**4**): 040203. DOI: 10.1088/1674-1056/ad21f4

Bifurcation and dynamics in double-delayed Chua circuits with periodic perturbation

Wenjie Yang(杨文杰)
Chin. Phys. B, 2022, 31 (**2**): 020201. DOI: 10.1088/1674-1056/ac1e0b

Magnetization relaxation of uniaxial anisotropic ferromagnetic particles with linear reaction dynamics driven by DC/AC magnetic field

Yu-Song Hu(胡玉松), Min Jiang(江敏), Tao Hong(洪涛), Zheng-Ming Tang(唐正明), and Ka-Ma Huang(黄卡玛)
Chin. Phys. B, 2021, 30 (**9**): 090202. DOI: 10.1088/1674-1056/abeb0b

Coexisting hidden attractors in a 4D segmented disc dynamo with one stable equilibrium or a line equilibrium

Jianghong Bao(鲍江宏), Dandan Chen(陈丹丹)
Chin. Phys. B, 2017, 26 (**8**): 080201. DOI: 10.1088/1674-1056/26/8/080201

Mechanism analysis of regulating Turing instability and Hopf bifurcation of malware propagation in mobile wireless sensor networks

Xi-Xi Huang(黄习习)[1], Min Xiao(肖敏)[1,†], Leszek Rutkowski[2], Hai-Bo Bao(包海波)[3], Xia Huang(黄霞)[3], and Jin-De Cao(曹进德)[4]

[1] *College of Automation & College of Artificial Intelligence, Nanjing University of Posts and Telecommunications, Nanjing* 210023, *China*
[2] *Systems Research Institute of the Polish Academy of Sciences*, 01-447 *Warsaw, Poland*
[3] *College of Electrical Engineering and Automation, Shandong University of Science and Technology, Qingdao* 266590, *China*
[4] *School of Mathematics, Southeast University, Nanjing* 210096, *China*

(Received 9 November 2023; revised manuscript received 19 January 2024; accepted manuscript online 1 February 2024)

A dynamical model is constructed to depict the spatial-temporal evolution of malware in mobile wireless sensor networks (MWSNs). Based on such a model, we design a hybrid control scheme combining parameter perturbation and state feedback to effectively manipulate the spatiotemporal dynamics of malware propagation. The hybrid control can not only suppress the Turing instability caused by diffusion factor but can also adjust the occurrence of Hopf bifurcation induced by time delay. Numerical simulation results show that the hybrid control strategy can efficiently manipulate the transmission dynamics to achieve our expected desired properties, thus reducing the harm of malware propagation to MWSNs.

Keywords: mobile wireless sensor networks, reaction-diffusion, Hopf bifurcation, hybrid control

PACS: 02.30.Jr, 02.60.Cb **DOI:** 10.1088/1674-1056/ad24d5

1. Introduction

Mobile wireless sensor networks (MWSNs) are composed of a large number of movable nodes.[1] Compared to static sensor networks, MWSNs have greater computing, communication and tracking capabilities.[2] Therefore, MWSNs have gained widespread attention in academic research and industrial fields.[3] A computer virus is a set of replicable and destructive instructions artificially injected into a code designed to destroy the data and functions of a computer, allowing it to run with large-scale replication and infection of other computers, resulting in network congestion, system paralysis, and even a threat to national security. Since most of the nodes of mobile wireless sensors are exposed to complex networks and are more vulnerable to various malicious signals, a cyber defense system is needed to protect the valuable information they store and transmit. Considering the similarity between network viruses and biological viruses, many scholars have used the theory of infectious disease to study the propagation process of malicious programs and construct a reasonable model of malicious program propagation, which can effectively safeguard the user's network environment and facilitate the prevention and control of network viruses.[4]

The propagation of malware leads to various dynamic behaviors, i.e., the behavior of the system switches between a stable equilibrium point and a stable limit ring when a parameter changes in a network node.[5,6] Such a dynamic evolution process is called Hopf bifurcation, which is a common nonlinear phenomenon. A supercritical bifurcation occurs when a limit loop exists with a parameter greater than the bifurcation value. On the contrary, a subcritical bifurcation occurs. Ren *et al.*[7] developed a model for SIR virus propagation considering the effect of antivirus capability and discussed the possible subcritical bifurcation behavior of the system. Chong *et al.*[8] proposed a discrete system with Allee effect. Using the central manifold theorem and bifurcation theory, they investigated various types of bifurcation behaviors of the system, including transcritical, pitchfork, and fold bifurcations. A tuberculosis transmission model was proposed by Abdelouahab.[9] It is found that the system exhibits saddle-knot bifurcations, i.e., transcritical bifurcations between equilibrium points, under different parameter controls. However, these models ignore the effect of time delay on virus propagation. In Ref. [10], a SLB computer virus propagation model is developed by considering the time delay caused by antivirus software to check and kill the virus. Yao *et al.*[11] proposed a worm propagation model with two time delays and a variable infection rate based on isolation strategy, and demonstrated that controlling the time delay within a certain range can effectively inhibit the spread of the worm.

These models assume that all individuals are stationary and only describe the temporal dynamics of malware in the network without considering its spatial distribution over time. So far, diffusion effects have been widely studied in neural network dynamics, but less studied in malicious virus propagation.[12] Kumari *et al.*[13] considered a malware propa-

†Corresponding author. E-mail: candymanxm2003@aliyun.com
© 2024 Chinese Physical Society and IOP Publishing Ltd

gation model with s-type removal rate and analyzed its spatio-temporal stability, as well as global stability. In addition, this paper introduces optimal control to inform how the virus propagation should be suppressed and eliminated.

In real life, Hopf bifurcations are mostly harmful dynamical behaviors; therefore, a controller needs to be designed to eliminate these harmful behaviors.[14] Currently, common controllers are proportional-integral-derivative (PID) control, proportional-derivative (PD) control, hybrid control, and so on.[15,16] Zhu *et al.*[17] introduced a state feedback controller for infected nodes in MWSNs. Hybrid control is a control method combining state feedback control and parameter regulation, generally applied to the Hopf bifurcation phenomenon in continuous nonlinear systems, and can be applied to higher-order systems by adjusting the control parameters to change the bifurcation threshold and stability of the system. Mao *et al.*[18] introduced a hybrid controller to a Hopfield neural networks model with time delays and verified through simulation that this control method is effective compared to other single control methods. Zhou *et al.*[19] investigated a delayed fractional-order predator-prey model and imposed hybrid control on mature predator populations, delaying the emergence of Hopf bifurcation and improving the stability of the system. However, hybrid controllers have been relatively little studied in malware propagation models.

In order to more thoroughly study the propagation dynamics of malware in MWSNS, this paper expands the current research from the time dimension to the spatio-temporal dimension and establishes a nonlinear reaction–diffusion model of malware propagation. Currently, most existing controllers are applied to systems described by ordinary differential equations, but we innovatively introduce a more general hybrid control into the reaction–diffusion malware propagation model. In addition, this paper considers the effects of virus latency time delay and recovery time delay simultaneously on the temporal and spatial evolution of viral transmission in MWSNs, gives the conditions for the occurrence of Turing instability and Hopf bifurcation, and compares the changes of system stability and bifurcation properties under the action of different controllers.

This article is structured as follows. In Section 2, we develop a nonlinear time delay malware propagation model and introduce a hybrid controller. The conditions for the occurrence of Turing instability and Hopf bifurcation are given in Section 3. In Section 4, the properties of Hopf bifurcation are analyzed using normal form theory and the center manifold theorem. Numerical simulations are given in Section 5 to verify the above conclusions. Section 6 gives the final conclusion of this paper.

2. Model formulation

A modified SIRS model was proposed by Fang *et al.*[20] as follows:

$$\begin{cases} \dfrac{\mathrm{d}S(t)}{\mathrm{d}t} = \mu N - \dfrac{\pi r^2}{L^2}\beta S(t)I(t) - (\mu+\omega)S + \varepsilon R, \\ \dfrac{\mathrm{d}I(t)}{\mathrm{d}t} = \dfrac{\pi r^2}{L^2}\beta S(t)I(t) - (\mu+\gamma)I, \\ \dfrac{\mathrm{d}R(t)}{\mathrm{d}t} = \omega S + \gamma I - (\mu+\varepsilon)R, \end{cases} \tag{1}$$

where $S(x,t)$, $I(x,t)$ and $R(x,t)$ represent susceptible, infected, and recovered nodes in a wireless sensor network, respectively. r is the node communication radius, L^2 is the node distribution range, β is the infection rate, and ε is the probability of a recovered node becoming susceptible again. ω and γ are the node conversion rates.

Based on the above ordinary differential equations, we extend this to the spatio-temporal domain. These nodes are randomly and evenly distributed in the two-dimensional region in MWSNs. Let $S(x,t)$, $I(x,t)$, $R(x,t)$ be the distribution density of susceptible, infected and removed nodes at time t and space location x, respectively. Considering the engineering significance of MWSNs, the attack and defense against malicious viruses should be completed in a very short time, otherwise the best time to protect information security will be lost. Therefore, the latency time delay and the infection time delay only have a very small numerical difference, so we use τ to describe these two time delays. Inspired by the literature,[21,22] the number of susceptible nodes that can be successfully infected by an infected node is $\frac{\pi r^2[1-(1-p)^\rho]}{L^2}S$, where r is the communication radius of each node, ρ is the node packet sending rate, and p is the successful packet delivery rate. Assuming $\Upsilon_1 = \pi r^2[1-(1-p)^\rho]/L^2$, in this paper, we adopt the nonlinear incidence $\Upsilon_2 SI/(1+bI)$ which is more in line with the characteristics of virus propagation, so that $\beta = \Upsilon_1\Upsilon_2$. Thus, we model the propagation of malware in MWSNs as follows:

$$\begin{cases} \dfrac{\partial S(x,t)}{\partial t} = d_1\Delta S(x,t) + A - \dfrac{\beta S(x,t)I(x,t-\tau)}{1+bI(x,t-\tau)} \\ \qquad\qquad - (\mu+\sigma)S(x,t), \\ \dfrac{\partial I(x,t)}{\partial t} = d_2\Delta I(x,t) + \dfrac{\beta S(x,t)I(x,t-\tau)}{1+bI(x,t-\tau)} \\ \qquad\qquad - \gamma I(x,t-\tau) - \mu I(x,t), \\ \dfrac{\partial R(x,t)}{\partial t} = d_3\Delta R(x,t) + \sigma S(x,t) + \gamma I(x,t-\tau) \\ \qquad\qquad - \mu R(x,t), \end{cases} \tag{2}$$

with Neumann boundary conditions and initial conditions

$$\frac{\partial S(x,t)}{\partial \eta} = \frac{\partial I(x,t)}{\partial \eta} = \frac{\partial R(x,t)}{\partial \eta} = 0, \quad x \in \partial\Omega, \quad t > 0,$$

$$\begin{cases} S(x,t) = S_0(x,t) \geq 0, \\ I(x,t) = I_0(x,t) \geq 0, \\ R(x,t) = R_0(x,t) \geq 0, \\ (x,t) \in \bar{\Omega} \times [-\tau, 0], \end{cases}$$

where A represents the newly added sensor nodes in the MWSNs, b is the half saturation constant of infected nodes, μ is the drop-out rate of nodes, σ is the immunization rate caused by the user's pre-installed anti-virus software, and γ is the rate of transferring infected nodes to the removed nodes. Ω delegates the network region, $\partial\Omega$ is the boundary of Ω, and η denotes the outside normal vector of $\partial\Omega$. $\Delta = \partial^2/\partial x^2$ is a Laplace operator in one dimension. The Neumann boundary condition $\partial S(x,t)/\partial\eta = \partial I(x,t)/\partial\eta = \partial R(x,t)/\partial\eta = 0$ indicates no communication between nodes across the boundaries. $S_0(x,t)$, $I_0(x,t)$ and $R_0(x,t)$ are nonnegative continuous functions.

In MWSNs, the periodic oscillations generated by Hopf bifurcation are known to affect the performance of nodes and even disrupt the normal operation of the entire network. Thus, it is necessary for us to introduce the hybrid controller into the model to suppress the generation of Hopf bifurcation. Hybrid control strategy is applied to the infected nodes of system (2), which is

$$k_1 F(x,t,\tau) + k_2[(I(x,t) - I^*) + (I(x,t) - I^*)^3],$$

where $F(x,t,\tau)$ is the right-hand end of the second equation of system (2), k_1 is the adjustable parameter, k_2 is the state feedback parameter, and I^* is the positive equilibrium steady state of infected nodes. Thus, the following controlled system can be obtained:

$$\begin{cases} \dfrac{\partial S(x,t)}{\partial t} = d_1 \Delta S(x,t) + A - \dfrac{\beta S(x,t) I(x,t-\tau)}{1 + bI(x,t-\tau)} \\ \qquad\qquad - (\mu + \sigma) S(x,t), \\ \dfrac{\partial I(x,t)}{\partial t} = k_1 [d_2 \Delta I(x,t) + \dfrac{\beta S(x,t) I(x,t-\tau)}{1 + bI(x,t-\tau)} \\ \qquad\qquad - \gamma I(x,t-\tau) - \mu I(x,t)] \\ \qquad\qquad + k_2[(I(x,t) - I^*) + (I(x,t) - I^*)^3], \\ \dfrac{\partial R(x,t)}{\partial t} = d_3 \Delta R(x,t) + \sigma S(x,t) + \gamma I(x,t-\tau) \\ \qquad\qquad - \mu R(x,t). \end{cases} \tag{3}$$

Remark 1 Many existing malware propagation models are based on ordinary differential equations (ODEs), which ignores an important factor: spatial factor. Change in the spatial location of nodes has an impact on the node density. Therefore, we introduce Laplace operators to represent the second order derivatives of spatial variables as a way to describe the spatial propagation behavior of malware.

Remark 2 Hybrid control has been successfully applied to control Hopf bifurcation of ODE systems.[23,24] We first adopt it to optimize the unfavorable spatiotemporal dynamics of malware propagation in MWSNs. The hybrid controller does not alter the position of equilibrium point of the original system (2), so that it realizes the control object without changing the properties of system (2).

3. Spatiotemporal dynamics analysis

Without considering the diffusion term, the virus-free equilibrium point $E_0 = (\frac{A}{\mu+\sigma}, 0, \frac{\sigma A}{\mu(\mu+\sigma)})$ and the endemic equilibrium point $E_1 = (S^*, I^*, R^*)$ of the controlled system (3) can be obtained, where

$$\begin{aligned} S^* &= \frac{bA + \mu + \gamma}{\beta + b(\mu + \sigma)}, \\ I^* &= \frac{A - (\mu + \sigma) S^*}{\mu + \gamma}, \\ R^* &= \frac{\sigma S^* + \gamma I^*}{\mu}. \end{aligned}$$

The basic reproduction number R_0 plays an important role in virus propagation studies.[25] In this paper, we use the regeneration matrix approach to calculate R_0. Let

$$\frac{\mathrm{d}f_i}{\mathrm{d}t} = \Sigma_i(x) - \Gamma_i(x), \quad i = 1, 2, \cdots m,$$

where $\Sigma_i(x)$ is the rate of individuals newly infected with the node in group i and $\Gamma_i(x)$ is the rate of removal. If the equilibrium point is $x_0 = \{x | x_i = 0, x = 1, 2, \ldots m\}$, then $\boldsymbol{F} = \left[\frac{\partial \Sigma_i}{\partial x_j}(x_0)\right]$, $\boldsymbol{V} = \left[\frac{\partial \Gamma_i}{\partial x_j}(x_0)\right]$, the regeneration matrix is denoted as $\boldsymbol{F}\boldsymbol{V}^{-1}$. R_0 is the spectral radius of the regeneration matrix $\rho(\boldsymbol{F}\boldsymbol{V}^{-1})$. Letting $\boldsymbol{X} = (I, R)$, from system (3), it is obtained that

$$\frac{\mathrm{d}\boldsymbol{X}}{\mathrm{d}t} = \boldsymbol{F} - \boldsymbol{V}, \tag{4}$$

where

$$\boldsymbol{F} = \begin{pmatrix} \dfrac{\beta S(x,t) I(x,t-\tau)}{1 + bI(x,t-\tau)} \\ \sigma S(x,t) + \gamma I(x,t-\tau) \end{pmatrix},$$
$$\boldsymbol{V} = \begin{pmatrix} \gamma I(x,t) + \mu I(x,t) \\ \mu R(x,t) \end{pmatrix}.$$

The Jacobian matrices at the virus-free equilibrium point E_0 respectively are

$$\boldsymbol{J}_F = \begin{pmatrix} \dfrac{\beta A}{\mu + \sigma} & 0 \\ \gamma & 0 \end{pmatrix}, \quad \boldsymbol{J}_V = \begin{pmatrix} \mu + \gamma & 0 \\ 0 & \mu \end{pmatrix}.$$

Hence, the basic reproduction number of system (3) is

$$R_0 = \rho(\boldsymbol{J}_F \boldsymbol{J}_V^{-1}) = \max_{\lambda \in \sigma(\boldsymbol{J}_F \boldsymbol{J}_V^{-1})} \{|\lambda|\} = \frac{\beta A}{(\mu + \sigma)(\mu + \gamma)},$$

where σ is the spectrum, i.e., the set consisting of all eigenvalues of the square matrix $\boldsymbol{F}\boldsymbol{V}^{-1}$.

Lemma 1 If $R_0 > 1$, then there is a unique endemic equilibrium point E_1 in the controlled system (3). If $R_0 < 1$, then the controlled system (3) has no endemic equilibrium point.

Proof When $R_0 > 1$, we get $\beta A > (\mu+\sigma)(\mu+\gamma)$, then $S^* > A/\beta > 0$. Considering $A-(\mu+\sigma)S^* = [\beta A-(\mu+\sigma)(\mu+\gamma)]/[\beta+b(\mu+\sigma)] > 0$, it is clear that $I^* > 0$ and $R^* > 0$. This indicates that the controlled system (3) has only one endemic equilibrium E_1. When $R_0 < 1$, we have $S^* > 0$, $I^* < 0$, in consequence the endemic equilibrium point does not exist.

Let $\tilde{S}(x,t) = S(x,t) - S^*$, $\tilde{I}(x,t) = I(x,t) - I^*$, $\tilde{R}(x,t) = R(x,t) - R^*$. Linearizing Eq. (3) at E_1, we can obtain

$$\begin{pmatrix} \dfrac{\partial \tilde{S}(x,t)}{\partial t} \\ \dfrac{\partial \tilde{I}(x,t)}{\partial t} \\ \dfrac{\partial \tilde{R}(x,t)}{\partial t} \end{pmatrix} = \boldsymbol{D}\Delta \begin{pmatrix} \tilde{S}(x,t) \\ \tilde{I}(x,t) \\ \tilde{R}(x,t) \end{pmatrix} + \boldsymbol{L}_1 \begin{pmatrix} \tilde{S}(x,t) \\ \tilde{I}(x,t) \\ \tilde{R}(x,t) \end{pmatrix} + \boldsymbol{L}_2 \begin{pmatrix} \tilde{S}(x,t-\tau) \\ \tilde{I}(x,t-\tau) \\ \tilde{R}(x,t-\tau) \end{pmatrix}, \tag{5}$$

where

$$\boldsymbol{D} = \mathrm{diag}\{d_1, d_2', d_3\},$$
$$\boldsymbol{L}_1 = \begin{pmatrix} a_{11} & 0 & 0 \\ a_{21} & a_{22} & 0 \\ a_{31} & 0 & a_{33} \end{pmatrix}, \quad \boldsymbol{L}_2 = \begin{pmatrix} 0 & b_{12} & 0 \\ 0 & b_{22} & 0 \\ 0 & b_{32} & 0 \end{pmatrix},$$

with

$$d_2' = k_1 d_2, \quad a_{11} = -\frac{\beta I^*}{1+bI^*} - \mu - \sigma, \quad a_{21} = k_1 \frac{\beta I^*}{1+bI^*},$$
$$a_{22} = -k_1\mu + k_2, \quad a_{31} = \sigma,$$
$$a_{33} = -\mu, \quad b_{12} = -\frac{\beta S^*}{(1+bI^*)^2},$$
$$b_{22} = k_1\left[\frac{\beta S^*}{(1+bI^*)^2} - \gamma\right], \quad b_{32} = \gamma.$$

The corresponding characteristic equation of system (3) is

$$\det(\lambda \boldsymbol{I} - \boldsymbol{M}_k - \boldsymbol{L}_1 - \boldsymbol{L}_2 \mathrm{e}^{-\lambda\tau}) = 0, \tag{6}$$

where $\boldsymbol{I}$ is a 3×3 identity matrix and $\boldsymbol{M}_k = -\boldsymbol{D}k^2, k \in \{0,1,2,\ldots\}$. Thus, Eq. (6) is equivalent to

$$\begin{aligned} 0 = {} & \lambda^3 + m_1(k^2,k_1,k_2)\lambda^2 + m_2(k^2,k_1,k_2)\lambda \\ & + m_3(k^2,k_1,k_2) + [l_1\lambda^2 + l_2(k^2,k_1,k_2)\lambda \\ & + l_3(k^2,k_1,k_2)]\mathrm{e}^{-\lambda\tau}, \end{aligned} \tag{7}$$

the corresponding coefficients are

$$\begin{aligned} m_1(k^2,k_1,k_2) &= d_1k^2 + d_2'k^2 + d_3k^2 - a_{11} - a_{22} - a_{33}, \\ m_2(k^2,k_1,k_2) &= (d_1k^2 - a_{11})(d_2'k^2 - a_{22}) + (d_3k^2 - a_{33}) \\ &\quad \times (d_1k^2 + d_2'k^2 - a_{11} - a_{22}), \\ m_3(k^2,k_1,k_2) &= (d_1k^2 - a_{11})(d_2'k^2 - a_{22})(d_3k^2 - a_{33}), \\ l_1 &= -b_{22}, \\ l_2(k^2,k_1,k_2) &= -b_{22}(d_1k^2 + d_3k^2 - a_{11} - a_{33}) - a_{21}b_{12}, \\ l_3(k^2,k_1,k_2) &= -b_{22}(d_1k^2 - a_{11})(d_3k^2 - a_{33}) \\ &\quad - a_{21}b_{12}(d_3k^2 - a_{33}). \end{aligned}$$

Next, we will analyze the Turing instability and Hopf bifurcation of system (3).

3.1. Turing instability

The mechanism of Turing is an instability caused by a diffusion term. In this subsection, the Turing instability of system (3) without time delay is studied.

When $\tau = 0$, $d_i = 0$ $(i = 1,2,3)$, $k_1 = 1$, $k_2 = 0$, Eq. (7) is simplified to

$$\lambda^3 + \varpi_1(k_1,k_2)\lambda^2 + \varpi_2(k_1,k_2)\lambda + \varpi_3(k_1,k_2) = 0, \tag{8}$$

with

$$\begin{aligned} \varpi_1(k_1,k_2) &= -a_{11} - a_{22} - a_{33} - b_{22}, \\ \varpi_2(k_1,k_2) &= a_{11}a_{22} + a_{33}(a_{11} + a_{22}) \\ &\quad + b_{22}(a_{11} + a_{33}) - a_{21}b_{12}, \\ \varpi_3(k_1,k_2) &= -a_{11}a_{22}a_{33} - a_{11}a_{33}b_{22} + a_{21}a_{33}b_{12}. \end{aligned}$$

Suppose that the following holds:

$$(H_1)\ \ \varpi_1(1,0) > 0,\ \varpi_2(1,0) > 0,\ \varpi_3(1,0) > 0,$$
$$\varpi_1(1,0)\varpi_2(1,0) - \varpi_3(1,0) > 0.$$

By virtue of the well-known Routh–Hurwitz criteria, when (H_1) holds, it can be concluded that all roots of Eq. (8) have negative real parts. Thus, the uncontrolled system (3) is locally asymptotically stable in the absence of time delay and diffusion term.

When $\tau = 0$, $d_i > 0$ $(i = 1,2,3)$, $k_1 = 1$, $k_2 = 0$, Eq. (7) becomes

$$0 = \lambda^3 + \chi_1(k^2,k_1,k_2)\lambda^2 + \chi_2(k^2,k_1,k_2)\lambda + \chi_3(k^2,k_1,k_2), \tag{9}$$

where

$$\begin{aligned} \chi_1(k^2,k_1,k_2) &= \chi_{11}(k_1)k^2 + \varpi_1(k_1,k_2), \\ \chi_2(k^2,k_1,k_2) &= \chi_{21}(k_1)k^4 + \chi_{22}(k_1,k_2)k^2 + \varpi_2(k_1,k_2), \\ \chi_3(k^2,k_1,k_2) &= \chi_{31}(k_1)k^6 + \chi_{32}(k_1,k_2)k^4 \\ &\quad + \chi_{33}(k_1,k_2)k^2 + \varpi_3(k_1,k_2), \end{aligned}$$

with

$$\begin{aligned} \chi_{11}(k_1) &= d_1 + d_2' + d_3 > 0, \\ \chi_{21}(k_1) &= d_1d_2' + d_1d_3 + d_2'd_3 > 0, \\ \chi_{22}(k_1,k_2) &= -a_{22}d_1 - a_{11}d_2' - d_3(a_{11} + a_{22}) \\ &\quad - a_{33}(d_1 + d_2') - b_{22}(d_1 + d_3), \\ \chi_{31}(k_1) &= d_1d_2'd_3 > 0, \end{aligned}$$

$$\begin{aligned}\chi_{32}(k_1,k_2) &= -a_{33}d_1d_2' - d_3(a_{22}d_1+a_{11}d_2) - b_{22}d_1d_3,\\ \chi_{33}(k_1,k_2) &= a_{33}(a_{22}d_1+a_{11}d_2) + a_{11}a_{22}d_3\\ &\quad + b_{22}(a_{33}d_1+a_{11}d_3) - a_{21}b_{12}d_3.\end{aligned}$$

Let $x=k^2$, we denote

$$\begin{aligned}&\mathcal{F}(x) = \chi_3(x,1,0)\\ &= \chi_{31}(1)x^3+\chi_{32}(1,0)x^2+\chi_{33}(1,0)x+\varpi_3(1,0). \quad (10)\end{aligned}$$

Make the following assumption:

$$(H_2)\ \ \chi_{33}(1,0)<0, \quad \mathcal{F}({x_2}^*)<0,$$

in which

$${x_2}^* = \frac{-\chi_{32}(1,0)+\sqrt{\chi_{32}^2(1,0)-3\chi_{31}(1)\chi_{33}(1,0)}}{3\chi_{31}(1)}.$$

Lemma 2 If (H_2) is satisfied, then $\mathcal{F}(x)=0$ has two positive roots x_1, x_2 $(x_1<x_2)$. Then, $\mathcal{F}(x)<0$ holds for $\forall x\in(x_1,x_2)$.

Proof When $\chi_{33}(1,0)<0$, $\mathcal{F}'(x)=3\chi_{31}(1)x^2+2\chi_{32}(1,0)x+\chi_{33}(1,0)$ has two positive roots

$${x_1}^* = (-\chi_{32}(1,0)-\sqrt{\chi_{32}^2(1,0)-3\chi_{31}(1)\chi_{33}(1,0)})/3\chi_{31}(1),$$

$${x_2}^* = (-\chi_{32}(1,0)+\sqrt{\chi_{32}^2(1,0)-3\chi_{31}(1)\chi_{33}(1,0)})/3\chi_{31}(1).$$

Since $\mathcal{F}(0)=\varpi_3(1,0)>0$, $\lim\limits_{x\to\infty}\mathcal{F}(x)=+\infty$, $\mathcal{F}({x_2}^*)<0$, $\mathcal{F}(x)=0$ always has two positive roots x_1 and x_2.

Define

$$h(\lambda;k)=\lambda^3+\chi_1(k^2,1,0)\lambda^2+\chi_2(k^2,1,0)\lambda+\chi_3(k^2,1,0).$$

Clearly, $\lim\limits_{\lambda\to\infty}h(\lambda;k)=+\infty$. We make the following assumption:

(H_3) There is a positive integer $k_0\in(x_1,x_2)$.

From Lemma 2, if $\varpi_3(1,0)>0$, (H_2) and (H_3) are satisfied, then $\mathcal{F}({k_0}^2)=\chi_3({k_0}^2,1,0)<0$. Obviously, $h(\lambda;k)=0$ has at least one positive root.

When $\tau=0$, $d_i>0$ $(i=1,2,3)$, $k_1\neq0,1$, $k_2\neq0$, the system changes to the form of Eq. (9). We assume that

$$\begin{aligned}&(H_4)\ \ \chi_{32}(k_1,k_2)>0,\ \ \chi_{33}(k_1,k_2)>0\\ &\quad \text{or}\ \ \chi_{32}(k_1,k_2)>0,\ \ \chi_{33}(k_1,k_2)<0,\ \ \mathcal{F}(x_2^*)>0.\end{aligned}$$

If (H_1) and (H_4) are satisfied, then $\mathcal{F}(x)>0$ holds for $\forall x>0$. Thus, we can get $\chi_3(k^2,k_1,k_2)>0$. After the above discussion, we have

$$\begin{aligned}&\chi_1(k^2,k_1,k_2)\chi_2(k^2,k_1,k_2)-\chi_3(k^2,k_1,k_2)\\ &=\hat{\chi}_1(k_1)k^6+\hat{\chi}_2(k_1,k_2)k^4+\hat{\chi}_3(k_1,k_2)k^2+\hat{\chi}_4(k_1,k_2),\end{aligned}$$

with

$$\begin{aligned}\hat{\chi}_1(k_1) &= \chi_{11}(k_1)\chi_{21}(k_1)-\chi_{31}(k_1)\\ &= {d_1}^2(d_2'+d_3)+{d_2'}^2(d_1+d_3)\\ &\quad +{d_3}^2(d_1+d_2')+2d_1d_2'd_3>0,\\ \hat{\chi}_2(k_1,k_2) &= \chi_{11}(k_1)\chi_{22}(k_1,k_2)\\ &\quad +\varpi_1(k_1,k_2)\chi_{21}(k_1)-\chi_{32}(k_1,k_2)\\ &= (d_1+d_2'+d_3)[-a_{22}d_1-a_{11}d_2'-d_3(a_{11}+a_{22})\\ &\quad -a_{33}(d_1+d_2')-b_{22}(d_1+d_3)]\\ &\quad -(a_{11}+a_{22}+a_{33}+b_{22})(d_1d_2'+d_1d_3+d_2'd_3)\\ &\quad +a_{33}d_1d_2'+d_3(a_{22}d_1+a_{11}d_2')+b_{22}d_1d_3,\\ \hat{\chi}_3(k_1,k_2) &= \varpi_2(k_1,k_2)\chi_{11}(k_1)\\ &\quad +\varpi_1(k_1,k_2)\chi_{22}(k_1,k_2)-\chi_{33}(k_1,k_2)\\ &= [a_{11}a_{22}+a_{33}(a_{11}+a_{22})](d_1+d_2'+d_3)\\ &\quad +[b_{22}(a_{11}+a_{33})-a_{21}b_{12}]\\ &\quad \times(d_1+d_2'+d_3)+(a_{11}+a_{22}+a_{33}+b_{22})\\ &\quad \times[a_{22}d_1+a_{11}d_2'+a_{11}d_3+a_{22}d_3]\\ &\quad +(-a_{11}-a_{22}-a_{33}-b_{22})\\ &\quad \times[-a_{33}(d_1+d_2')-b_{22}(d_1+d_3)]\\ &\quad -a_{33}(a_{22}d_1+a_{11}d_2')-a_{11}a_{22}a_{33}\\ &\quad -b_{22}(a_{33}d_1+a_{11}d_3)+a_{21}b_{12}d_3,\\ \hat{\chi}_4(k_1,k_2) &= \varpi_1(k_1,k_2)\varpi_2(k_1,k_2)-\varpi_3(k_1,k_2).\end{aligned}$$

Combining with (H_4), we know that $\hat{\chi}_4>0$. Make the following assumption:

$$(H_5)\hat{\chi}_2(k_1,k_2)>0, \quad \hat{\chi}_3(k_1,k_2)>0.$$

According to the Routh–Hurwitz criterion, if (H_1), (H_4) and (H_5) hold, then the roots of Eq. (9) have negative real parts. Consequently, system (2) is locally asymptotically stable.

Theorem 1 Assume that $R_0>1$, $\tau=0$ and (H_1) hold. We can draw the following conclusions.

1. If $d_i=0$ $(i=1,2,3)$, $k_1=1$, $k_2=0$ hold, then the uncontrolled system (2) is locally asymptotically stable.

2. If $d_i>0$ $(i=1,2,3)$, $k_1=1$, $k_2=0$, (H_2) and (H_3) hold, then the uncontrolled system (2) occurs Turing instability at E_1.

3. If $d_i>0$ $(i=1,2,3)$, $k_1\neq0,1$, $k_2\neq0$, (H_4) and (H_5) hold, then the controlled system (3) can return to a steady state under hybrid control.

Remark 3 From Theorem 1, it can be seen that Turing instability occurs when the diffusion coefficient meets certain conditions when no control is applied to the system. When the hybrid controller is added, the system returns to a stable state. It can be seen that the hybrid control can suppress the occurrence of Turing instability and improve the stability of the system.

3.2. Hopf bifurcation

If $\tau = 0$, $d_i > 0$, from the above discussion, it is clear to see that the controlled system (3) is locally asymptotically stable when (H_1), (H_4) and (H_5) hold.

For $\tau > 0$, $d_i > 0$, we assume that $\lambda = \mathrm{i}w$ $(w > 0)$ is the root of Eq. (7). We substitute it into Eq. (7) and separate the virtual and real parts yields

$$\begin{cases} \sin w\tau = \dfrac{l_2(k^2,k_1,k_2)w[m_1(k^2,k_1,k_2)w^2 - m_3(k^2,k_1,k_2)]}{[l_2(k^2,k_1,k_2)w]^2 + [l_1w^2 - l_3(k^2,k_1,k_2)]^2} \\ \qquad + \dfrac{[l_1w^2 - l_3(k^2,k_1,k_2)][w^3 - m_2(k^2,k_1,k_2)w]}{[l_2(k^2,k_1,k_2)w]^2 + [l_1w^2 - l_3(k^2,k_1,k_2)]^2}, \\ \cos w\tau = \dfrac{[-m_1(k^2,k_1,k_2)w^2 + m_3(k^2,k_1,k_2)]l_1w^2}{[l_2(k^2,k_1,k_2)w]^2 + [l_1w^2 - l_3(k^2,k_1,k_2)]^2} \\ \qquad + \dfrac{l_2(k^2,k_1,k_2)w[w^3 - m_2(k^2,k_1,k_2)w]}{[l_2(k^2,k_1,k_2)w]^2 + [l_1w^2 - l_3(k^2,k_1,k_2)]^2} \\ \qquad - \dfrac{[-m_1(k^2,k_1,k_2)w^2 + m_3(k^2,k_1,k_2)]l_3(k^2,k_1,k_2)}{[l_2(k^2,k_1,k_2)w]^2 + [l_1w^2 - l_3(k^2,k_1,k_2)]^2}, \end{cases} \tag{11}$$

from which we can obtain a sextic equation for w:

$$\begin{aligned} 0 \;=\; & w^6 + C_1(k^2,k_1,k_2)w^4 + C_2(k^2,k_1,k_2)w^2 \\ & + C_3(k^2,k_1,k_2), \end{aligned} \tag{12}$$

where the coefficients are

$$\begin{aligned} C_1(k^2,k_1,k_2) \;=\; & m_1^2(k^2,k_1,k_2) - {l_1}^2 - 2m_2(k^2,k_1,k_2), \\ C_2(k^2,k_1,k_2) \;=\; & m_2^2(k^2,k_1,k_2) - 2m_1(k^2,k_1,k_2)m_3(k^2,k_1,k_2) \\ & - l_2^2(k^2,k_1,k_2) + 2l_1l_3(k^2,k_1,k_2), \\ C_3(k^2,k_1,k_2) \;=\; & m_3^2(k^2,k_1,k_2) - l_3^2(k^2,k_1,k_2). \end{aligned}$$

Letting $z = w^2$, Eq. (12) is equivalent to a cubic equation with respect to z as follows:

$$0 = z^3 + C_1(k^2,k_1,k_2)z^2 + C_2(k^2,k_1,k_2)z + C_3(k^2,k_1,k_2). \tag{13}$$

When $k = 0$, Eq. (13) has at least one positive root if the following condition holds:

$$(H_6)\;\; C_3(0,k_1,k_2) = m_3^2(0,k_1,k_2) - l_3^2(0,k_1,k_2) < 0.$$

Without losing of generality, we assume that Eq. (13) has three positive roots z_n $(n = 1,2,3)$, then Eq. (12) has three positive roots $w_n = \sqrt{z_n}$ $(n = 1,2,3)$. By Eq. (11), we obtain

$$\begin{aligned} \tau_n^j \;=\; & \frac{\arccos \dfrac{L_4(k_1,k_2){w_n}^4 + L_5(k_1,k_2){w_n}^2 + L_6(k_1,k_2)}{L_1(k_1,k_2){w_n}^4 + L_2(k_1,k_2){w_n}^2 + L_3(k_1,k_2)}}{w_n} \\ & + \frac{2\pi j}{w_n}, \quad j = 0,1\ldots, \end{aligned} \tag{14}$$

where

$$\begin{aligned} L_1(k_1,k_2) \;=\; & {l_1}^2, \\ L_2(k_1,k_2) \;=\; & {l_2}^2(0,k_1,k_2) - 2l_1l_3(0,k_1,k_2), \\ L_3(k_1,k_2) \;=\; & {l_3}^2(0,k_1,k_2), \\ L_4(k_1,k_2) \;=\; & l_2(0,k_1,k_2) - m_1(0,k_1,k_2)l_1, \\ L_5(k_1,k_2) \;=\; & m_1(0,k_1,k_2)l_3(0,k_1,k_2) + l_1m_3(0,k_1,k_2) \\ & - m_2(0,k_1,k_2)l_2(0,k_1,k_2), \\ L_6(k_1,k_2) \;=\; & -m_3(0,k_1,k_2)l_3(0,k_1,k_2). \end{aligned}$$

Remark 4 Referring to Refs. [26,27], in Eq. (14), j represents the periodicity of the bifurcation point, which is the minimum bifurcation point when $j = 0$.

Define

$$\tau_0 = \tau_{n_0}^0 = \min_{n\in\{1,2,3\}}\{\tau_n^0\}, \quad w_0 = w_{n_0}.$$

Denote

$$\begin{aligned} h_1(y,k_1,k_2) \;=\; & {m_1}^2(y,k_1,k_2) - 2m_2(y,k_1,k_2) - {l_1}^2, \\ h_2(y,k_1,k_2) \;=\; & {m_2}^2(y,k_1,k_2) - 2m_1(y,k_1,k_2)m_3(y,k_1,k_2) \\ & - {l_2}^2(y,k_1,k_2) + 2l_1l_3(y,k_1,k_2), \\ h_3(y,k_1,k_2) \;=\; & m_3^2(y,k_1,k_2) - {l_3}^2(y,k_1,k_2). \end{aligned}$$

Make the following hypotheses:

$$(H_7)\quad h_i'(y,k_1,k_2) > 0, \;\; \text{for} \;\; y \geq 1, \;\; i = 1,2,3,\ldots.$$

Under (H_7), $h_i(y)$ $(i = 1,2,3)$ is monotonically increasing when $y \geq 1$. Thus

$$\begin{aligned} h_1(y,k_1,k_2) \;\geq\; & {m_1}^2(1,k_1,k_2) - 2m_2(1,k_1,k_2) - {l_1}^2, \\ h_2(y,k_1,k_2) \;\geq\; & {m_2}^2(1,k_1,k_2) - 2m_1(1,k_1,k_2)m_3(1,k_1,k_2) \\ & - {l_2}^2(1,k_1,k_2) + 2l_1l_3(1,k_1,k_2), \\ h_3(y,k_1,k_2) \;\geq\; & m_3^2(1,k_1,k_2) - {l_3}^2(1,k_1,k_2). \end{aligned}$$

Make the following assumptions:

$$\begin{aligned} &(H_8)\quad {m_1}^2(1,k_1,k_2) - 2m_2(1,k_1,k_2) - {l_1}^2 > 0, \\ &(H_9)\quad {m_2}^2(1,k_1,k_2) - 2m_1(1,k_1,k_2)m_3(1,k_1,k_2) \\ &\qquad - {l_2}^2(1,k_1,k_2) + 2l_1l_3(1,k_1,k_2) > 0, \\ &(H_{10})\quad {m_3}^2(1,k_1,k_2) - {l_3}^2(1,k_1,k_2) > 0. \end{aligned}$$

From (H_7)–(H_{10}), it follows that

$$C_i(k^2,k_1,k_2) = h_i(y,k_1,k_2) \geq h_i(1,k_1,k_2) > 0.$$

Thus, Eq. (12) has no positive real roots. Below we verify the transversality condition when $k = 0$. Differentiating both sides of Eq. (7) with respect to τ, one can get

$$\left(\frac{\mathrm{d}\lambda}{\mathrm{d}\tau}\right)^{-1} = \frac{S_1(\lambda)}{S_2(\lambda)} - \frac{\tau}{\lambda},$$

where

$$\begin{aligned} S_1(\lambda) \;=\; & 3\lambda^2 + 2m_1(0,k_1,k_2)\lambda + m_2(0,k_1,k_2) \\ & + (2l_1\lambda + l_2(0,k_1,k_2))\,\mathrm{e}^{-\lambda\tau}, \\ S_2(\lambda) \;=\; & \mathrm{e}^{-\lambda\tau}(l_1\lambda^3 + l_2(0,k_1,k_2)\lambda^2 + l_3(0,k_1,k_2\lambda)). \end{aligned}$$

Let $\lambda=\alpha(\tau)+\mathrm{i}w(\tau)$ be the root of Eq. (7) near $\tau=\tau_0$ satisfying $\alpha(\tau_0)=0$, $w(\tau_0)=w_0$. Then

$$S_1(\lambda)=M_1+\mathrm{i}M_2,$$
$$S_2(\lambda)=N_1+\mathrm{i}N_2,$$

where

$$\begin{aligned}
M_1 &= -3{w_0}^2+m_2(0,k_1,k_2)+2l_1w_0\sin w_0\tau_0\\
&\quad +l_2(0,k_1,k_2)\cos w_0\tau_0,\\
M_2 &= 2m_1(0,k_1,k_2)w_0+2l_1w_0\cos w_0\tau_0\\
&\quad -l_2(0,k_1,k_2)\sin w_0\tau_0,\\
N_1 &= -l_2(0,k_1,k_2){w_0}^2\cos w_0\tau_0\\
&\quad -l_1{w_0}^3\sin w_0\tau_0+l_3(0,k_1,k_2)w_0\sin w_0\tau_0,\\
N_2 &= -l_1{w_0}^3\cos w_0\tau_0+l_3(0,k_1,k_2)w_0\cos w_0\tau_0\\
&\quad +l_2(0,k_1,k_2){w_0}^2\sin w_0\tau_0,
\end{aligned}$$

thus the following expression is obtained:

$$\mathrm{Re}\left\{\frac{\mathrm{d}\lambda}{\mathrm{d}\tau}\right\}^{-1}_{\tau=\tau_0}=\mathrm{Re}\left\{\frac{M_1+\mathrm{i}M_2}{N_1+\mathrm{i}N_2}+\frac{\mathrm{i}\tau_0}{w_0}\right\}=\frac{M_1N_1+M_2N_2}{N_1^2+N_2^2}.$$

Note that

$$\mathrm{sign}\left\{\mathrm{Re}\left(\frac{\mathrm{d}\lambda}{\mathrm{d}\tau}\right)_{\tau=\tau_0}\right\}=\mathrm{sign}\left\{\mathrm{Re}\left(\frac{\mathrm{d}\lambda}{\mathrm{d}\tau}\right)^{-1}_{\tau=\tau_0}\right\}.$$

We make the following assumption:

$$(H_{11})\quad M_1N_1+M_2N_2>0.$$

If (H_{11}) holds, then $\mathrm{Re}(\mathrm{d}\lambda/\mathrm{d}\tau)^{-1}{}_{\tau=\tau_0}>0$. Combining the above discussion, it is easy to get the following theorem.

Theorem 2 Assume that $R_0>1$, $d_i>0$ $(i=1,2,3)$, (H_1) and (H_6)–(H_{11}) hold. We have reached the following conclusions.

1. The controlled system (3) is locally asymptotically stable for $\tau\in(0,\tau_0]$.

2. The controlled system (3) undergoes a Hopf bifurcation at E_1 when $\tau=\tau_0$.

Remark 5 From the expression of τ_0, we can see that its value is related to k_1 and k_2, so changing the values of k_1 and k_2 can adjust the bifurcation threshold of the system while keeping other parameters constant.

4. Direction and stability of the Hopf bifurcation

There are many methods for Hopf bifurcation study, including the Lyapunov–Schmidt method,[28] Lyapunov constant method,[29] averaging method, and so on. Here, we adopt the normal form and center manifold theory, which approximates the high-dimensional system to a two-dimensional plane by the central manifold theorem, and then transforms this two-dimensional system to a PB regular form by an approximate constant transformation, and finally relies on the discussion of the PB regular form to obtain the periodicity relation of the extremal ring, which can be used to discriminate the type of Hopf bifurcation.[30] Compared with other methods, this method by reducing the dimensionality of the system greatly simplifies the difficulty of dealing with the problem, and it is a mainstream method to deal with the bifurcation problem at present. The calculation of the direction of bifurcation is very complicated. We will give the detailed steps of the derivation process below.

Inspired by Refs. [31–33], we introduce a new variable $\delta=\tau-\tau^*$, where τ_0 is denoted by τ^*. The system (3) is transformed into a generalized differential equation at $\ell=C([-1,0],X)$ written in the following form by normalizing the time delay τ through the time-scaling $t\to t/\tau$:

$$\frac{\mathrm{d}\boldsymbol{U}(t)}{\mathrm{d}\boldsymbol{t}}=\tau^*\boldsymbol{D}\Delta\boldsymbol{U}(t)+\boldsymbol{L}(\tau^*)(\boldsymbol{U}_t)+\boldsymbol{F}(\boldsymbol{U}_t,\delta),\tag{15}$$

where $\boldsymbol{U}(x,t)=(S(x,t),I(x,t),R(x,t))^{\mathrm{T}}\in X$, $\boldsymbol{U}(t)\in\ell$. Otherwise, $\boldsymbol{L}(\tau^*)(\eta):C\to X$ and $\boldsymbol{F}(\cdot,\delta):C\to X$ are given by

$$\boldsymbol{L}(\tau^*)(\eta)=\tau^*\begin{pmatrix}a_{11}\eta_1(0)+b_{12}\eta_2(-1)\\ a_{21}\eta_1(0)+a_{22}\eta_2(0)+b_{22}\eta_2(-1)\\ a_{31}\eta_1(0)+b_{32}\eta_2(-1)+a_{33}\eta_3(0)\end{pmatrix},$$
$$\boldsymbol{F}(\eta,\delta)=\delta\boldsymbol{D}\Delta\eta(0)+\boldsymbol{L}(\delta)\eta+\boldsymbol{f}(\eta,\delta),$$

where

$$\boldsymbol{f}(\eta,\delta)=(\tau^*+\delta)\begin{pmatrix}V_1\\ V_2\\ 0\end{pmatrix},\tag{16}$$

in which

$$\begin{aligned}
V_1 &= a_{14}\eta_1(0)\eta_2(-1)+a_{15}{\eta_2}^2(-1)\\
&\quad +a_{16}\eta_1(0){\eta_2}^2(-1)+a_{17}{\eta_2}^3(-1),\\
V_2 &= a_{24}\eta_1(0)\eta_2(-1)+a_{25}{\eta_2}^2(-1)\\
&\quad +a_{26}\eta_1(0){\eta_2}^2(-1)+a_{27}{\eta_2}^3(-1)+k_2\eta_2^3(0),
\end{aligned}$$

with

$$a_{14}=-\frac{\beta}{(1+bI^*)^2},\quad a_{15}=\frac{\beta bS^*}{(1+bI^*)^3},\quad a_{16}=\frac{\beta b}{(1+bI^*)^3},$$
$$a_{17}=-\frac{\beta b^2S^*}{(1+bI^*)^4},\quad a_{24}=-k_1a_{14},\quad a_{25}=-k_1a_{15},$$
$$a_{26}=-k_1a_{16},\quad a_{27}=-k_1a_{17},$$

for $\boldsymbol{\eta}=(\eta_1,\eta_2,\eta_3)^{\mathrm{T}}\in\ell$.[34] The linearized of system (3) at $(0,0,0)^{\mathrm{T}}$ is

$$\frac{\mathrm{d}\boldsymbol{U}(t)}{\mathrm{d}t}=\tau^*\boldsymbol{D}\Delta\boldsymbol{U}(t)+\boldsymbol{L}(\tau^*)(\boldsymbol{U}_t).\tag{17}$$

From the previous discussions, we know that for $\tau=\tau^*$ the characteristic equation of Eq. (15) has a pair of simple purely imaginary eigenvalues $\boldsymbol{\Lambda}_0=\{-\mathrm{i}w_0\tau^*,\mathrm{i}w_0\tau^*\}$. By the Riesz

representation theorem, there exists a 3×3 matrix function $\boldsymbol{\Gamma}(\theta,\tau^*)(-1\le\theta\le 0)$ so that

$$-\tau^*\boldsymbol{D}k^2\eta(0)+\boldsymbol{L}(\tau^*)(\eta)=\int_{-1}^{0}[\mathrm{d}\boldsymbol{\Gamma}(\theta,\tau^*)]\eta(\theta). \quad (18)$$

In fact, for $\eta\in\ell$, we choose

$$\begin{aligned}\boldsymbol{\Gamma}(\theta,\tau^*) &= \tau^*\begin{pmatrix} a_{11}-d_1k^2 & 0 & 0\\ a_{21} & a_{22}-d_2'k^2 & 0\\ a_{31} & 0 & a_{33}-d_3k^2\end{pmatrix}\cdot\nu(\theta)\\ &\quad+\tau^*\begin{pmatrix}0 & -b_{12} & 0\\ 0 & -b_{22} & 0\\ 0 & -b_{32} & 0\end{pmatrix}\nu(\theta+1), \end{aligned}\quad (19)$$

where ν is the Dirac delta function that $\nu(0)=1$ and $\nu(\theta)=0$ $(-1\le\theta<0)$.[35] Let $\boldsymbol{A}(\tau^*)$ denote the infinitesimal generator of the semigroup and $\boldsymbol{A}^*$ be the formal adjoint of $\boldsymbol{A}(\tau^*)$ under the bilinear pairing

$$\begin{aligned}\langle\psi,\phi\rangle &= \psi(0)\phi(0)-\int_{-1}^{0}\int_{\zeta=0}^{0}\psi(\zeta-\theta)\mathrm{d}\boldsymbol{\Gamma}(\theta)\phi(\zeta)\mathrm{d}\zeta\\ &= \psi(0)\phi(0)+\tau^*\int_{-1}^{0}\psi(\theta+1)\begin{pmatrix}0 & b_{12} & 0\\ 0 & b_{22} & 0\\ 0 & b_{32} & 0\end{pmatrix}\phi(\theta)\mathrm{d}\theta,\end{aligned}\quad (20)$$

for $\phi\in C$, $\psi\in C([-1,0],X)$. From the above discussions, we know that $\pm\mathrm{i}w_0\tau^*$ are a pair of simple purely imaginary eigenvalues of $\boldsymbol{A}(\tau^*)$ and $\boldsymbol{A}^*(\tau^*)$. Let P and P^* represent the central subspace of $\boldsymbol{A}(\tau^*)$ and $\boldsymbol{A}^*(\tau^*)$ with respect to the eigenvalue $\boldsymbol{\Lambda}_0$, respectively. Suppose that $\boldsymbol{p}_1(\theta)=\mathrm{e}^{\mathrm{i}w_0\tau^*\theta}(1,\xi,\zeta)^{\mathrm{T}},(-1\le\theta\le 0)$, $\boldsymbol{p}_2(\theta)=\bar{\boldsymbol{p}}_1(\theta)$, $\boldsymbol{q}_1(s)=\mathrm{e}^{-\mathrm{i}w_0\tau^*s}(1,\xi^*,\zeta^*),(0\le s\le 1)$ and $\boldsymbol{q}_2(s)=\bar{\boldsymbol{q}}_1(s)$.[36] We derive

$$\begin{aligned}&(\lambda\boldsymbol{I}-\boldsymbol{A})\boldsymbol{p}_1(0)=0|_{\lambda=\mathrm{i}w_0\tau^*},\\ &(\lambda\boldsymbol{I}-\boldsymbol{A}^{\mathrm{T}})\boldsymbol{q}_1(0)=0|_{\lambda=-\mathrm{i}w_0\tau^*}.\end{aligned}$$

Then, we can easily obtain

$$\begin{aligned}&\xi=\frac{\mathrm{i}w_0+d_1k^2-a_{11}}{b_{12}\mathrm{e}^{-\mathrm{i}w_0\tau^*}},\\ &\xi^*=-\frac{\mathrm{i}w_0+a_{11}-d_1k^2}{a_{21}},\\ &\zeta=\frac{a_{31}b_{12}+b_{32}(\mathrm{i}w_0+d_1k^2-a_{11})}{b_{12}(\mathrm{i}w_0+d_3k^2-a_{33})},\quad \zeta^*=0.\end{aligned}\quad (21)$$

Let $\boldsymbol{\Omega}=(\boldsymbol{\Omega}_1,\boldsymbol{\Omega}_2)$, $\boldsymbol{\Omega}^*=(\boldsymbol{\Omega}_1^*,\boldsymbol{\Omega}_2^*)^{\mathrm{T}}$, for $\theta\in[-1,0]$. We have

$$\begin{aligned}\boldsymbol{\Omega}_1(\theta) &= \frac{\boldsymbol{p}_1(\theta)+\boldsymbol{p}_2(\theta)}{2}=\begin{pmatrix}\mathrm{Re}\{\mathrm{e}^{\mathrm{i}w_0\tau^*\theta}\}\\ \mathrm{Re}\{\xi\,\mathrm{e}^{\mathrm{i}w_0\tau^*\theta}\}\\ \mathrm{Re}\{\zeta\,\mathrm{e}^{\mathrm{i}w_0\tau^*\theta}\}\end{pmatrix}\\ &=\begin{pmatrix}\cos w_0\tau^*\theta\\ K_1\\ \dfrac{Y_1+Y_2}{-b_{12}[w_0^2+(a_{33}-d_3k^2)^2]}\end{pmatrix},\end{aligned}$$

$$\begin{aligned}\boldsymbol{\Omega}_2(\theta) &= \frac{\boldsymbol{p}_1(\theta)-\boldsymbol{p}_2(\theta)}{2\mathrm{i}}=\begin{pmatrix}\mathrm{Im}\{\mathrm{e}^{\mathrm{i}w_0\tau^*\theta}\}\\ \mathrm{Im}\{\xi\,\mathrm{e}^{\mathrm{i}w_0\tau^*\theta}\}\\ \mathrm{Im}\{\zeta\,\mathrm{e}^{\mathrm{i}w_0\tau^*\theta}\}\end{pmatrix}\\ &=\begin{pmatrix}\sin w_0\tau^*\theta\\ K_2\\ \dfrac{Y_3+Y_4}{-b_{12}[w_0^2+(a_{33}-d_3k^2)^2]}\end{pmatrix},\end{aligned}$$

for $\theta\in[-1,0]$, where

$$\begin{aligned}K_1 &= \frac{1}{b_{12}}[w_0\sin(w_0\tau^*-w_0\tau^*\theta)\\ &\quad+(d_1k^2-a_{11})\cos(w_0\tau^*-w_0\tau^*\theta)],\\ K_2 &= \frac{1}{b_{12}}[w_0\cos(w_0\tau^*-w_0\tau^*\theta)\\ &\quad-(d_1k^2-a_{11})\sin(w_0\tau^*-w_0\tau^*\theta)],\\ Y_1 &= \cos w_0\tau^*\theta[-a_{31}b_{12}(d_3k^2-a_{33})(d_1k^2-a_{11})],\\ Y_2 &= -w_0a_{31}b_{12}\sin w_0\tau^*\theta,\\ Y_3 &= \cos w_0\tau^*\theta[w_0a_{31}b_{12}+w_0b_{32}(d_1k^2-a_{11})\\ &\quad-w_0b_{32}(d_3k^2-a_{33})],\\ Y_4 &= \sin w_0\tau^*\theta[-a_{31}b_{12}(d_3k^2-a_{33})\\ &\quad-w_0^2b_{32}-b_{32}(d_1k^2-a_{11})(d_3k^2-a_{33})],\end{aligned}$$

and

$$\begin{aligned}\boldsymbol{\Omega}_1{}^*(s) &= \frac{\boldsymbol{q}_1(s)+\boldsymbol{q}_2(s)}{2}=\begin{pmatrix}\mathrm{Re}\{\mathrm{e}^{-\mathrm{i}w_0\tau^*s}\}\\ \mathrm{Re}\{\xi^*\mathrm{e}^{-\mathrm{i}w_0\tau^*s}\}\\ \mathrm{Re}\{\zeta^*\mathrm{e}^{-\mathrm{i}w_0\tau^*s}\}\end{pmatrix}^{\mathrm{T}}\\ &=\begin{pmatrix}\cos w_0\tau^*s\\ \dfrac{(a_{11}-d_1k^2)\cos w_0\tau^*s+w_0\sin w_0\tau^*s}{a_{21}}\\ 0\end{pmatrix}^{\mathrm{T}},\\ \boldsymbol{\Omega}_2{}^*(s) &= \frac{\boldsymbol{q}_1(s)-\boldsymbol{q}_2(s)}{2\mathrm{i}}=\begin{pmatrix}\mathrm{Im}\{\mathrm{e}^{-\mathrm{i}w_0\tau^*s}\}\\ \mathrm{Im}\{\xi^*\mathrm{e}^{-\mathrm{i}w_0\tau^*s}\}\\ \mathrm{Im}\{\zeta^*\mathrm{e}^{-\mathrm{i}w_0\tau^*s}\}\end{pmatrix}^{\mathrm{T}}\\ &=\begin{pmatrix}-\sin w_0\tau^*s\\ -\dfrac{(d_1k^2-a_{11})\sin w_0\tau^*s+w_0\cos w_0\tau^*s}{a_{21}}\\ 0\end{pmatrix}^{\mathrm{T}},\end{aligned}$$

for $s\in[-1,0]$. Note that

$$\begin{aligned}(\boldsymbol{q}_1,\boldsymbol{p}_1) &= (\boldsymbol{\Omega}_1{}^*,\boldsymbol{\Omega}_1)-(\boldsymbol{\Omega}_2{}^*,\boldsymbol{\Omega}_2)+\mathrm{i}[(\boldsymbol{\Omega}_1{}^*,\boldsymbol{\Omega}_2)+(\boldsymbol{\Omega}_2{}^*,\boldsymbol{\Omega}_1)],\\ (\boldsymbol{q}_1,\boldsymbol{p}_1) &= 1+\xi\xi^*+\zeta\zeta^*+\tau^*\xi\,\mathrm{e}^{\mathrm{i}w_0\tau^*}(b_{12}+b_{22}\xi^*+b_{32}\zeta^*)\\ &= \Xi^*.\end{aligned}$$

Then, we have

$$\begin{aligned}&(\boldsymbol{\Omega}_1^*,\boldsymbol{\Omega}_1)-(\boldsymbol{\Omega}_2^*,\boldsymbol{\Omega}_2)=\mathrm{Re}\{\Xi^*\},\\ &(\boldsymbol{\Omega}_1^*,\boldsymbol{\Omega}_2)+(\boldsymbol{\Omega}_2^*,\boldsymbol{\Omega}_1)=\mathrm{Im}\{\Xi^*\}.\end{aligned}$$

Next, we denote $(\boldsymbol{\Omega}^*,\boldsymbol{\Omega})=(\boldsymbol{\Omega}_j{}^*,\boldsymbol{\Omega}_k)$ $(j,k=1,2)$ and construct a new basis $\boldsymbol{\Psi}=(\boldsymbol{\Psi}_1,\boldsymbol{\Psi}_2,\boldsymbol{\Psi}_3)^{\mathrm{T}}=(\boldsymbol{\Omega}^*,\boldsymbol{\Omega})^{-1}\boldsymbol{\Omega}^*$.[37] Then, $(\boldsymbol{\Psi},\boldsymbol{\Phi})$ is a second order identity matrix. In addition,

define $\boldsymbol{f_k}=(\beta_k^1,\beta_k^2,\beta_k^3)$ and $\boldsymbol{\partial}\cdot f_0=\boldsymbol{\partial}_1\beta_k^1+\boldsymbol{\partial}_2\beta_k^2+\boldsymbol{\partial}_3\beta_k^3$ for $\boldsymbol{\partial}=(\boldsymbol{\partial}_1,\boldsymbol{\partial}_2,\boldsymbol{\partial}_3)^{\mathrm{T}}$, $\boldsymbol{\partial}_j\in R\ (j=1,2,3)$, where

$$\beta_k^1=\begin{pmatrix}\cos kx\\0\\0\end{pmatrix},\quad \beta_k^2=\begin{pmatrix}0\\\cos kx\\0\end{pmatrix},\ \beta_k^3=\begin{pmatrix}0\\0\\\cos kx\end{pmatrix}.$$

Then, the central subspace of the linearized system (17) is given by $P_{\mathrm{CN}}\ell$, where

$$P_{\mathrm{CN}}\ell(\eta)=\boldsymbol{\Omega}(\boldsymbol{\Psi},\langle\eta,\boldsymbol{f_k}\rangle)\cdot\boldsymbol{f_k},\quad \eta\in\ell, \tag{22}$$

and $\ell=P_{\mathrm{CN}}\ell+P_{\mathrm{S}}\ell$, where $P_{\mathrm{S}}\ell$ denotes the complementary subspace of $P_{\mathrm{CN}}\ell$. Define $\boldsymbol{A}(\tau^*)$ as

$$\boldsymbol{A}_{\tau^*}\eta(\theta)=\dot\eta(\theta)+\boldsymbol{X}_0(\theta)[\tau^*\boldsymbol{D}\Delta\eta(0)+\boldsymbol{L}(\tau^*)(\eta(\theta))-\dot\eta(0)]$$

for $\eta\in\ell\times X$, where

$$\boldsymbol{X}_0(\theta)=\begin{cases}0, & -1\le\theta<0,\\ I, & \theta=0.\end{cases}$$

Therefore, system (15) can be converted into the following abstract ordinary differential equation:

$$\dot{\boldsymbol{U}}_t=\boldsymbol{A}_{\tau^*}\boldsymbol{U}_t+\boldsymbol{X}_0\boldsymbol{F}(\boldsymbol{U}_t,\delta). \tag{23}$$

Using the decomposition $\ell=P_{\mathrm{CN}}\ell+P_{\mathrm{S}}\ell$ and Eq. (22), the solution of Eq. (23) can be written as

$$\boldsymbol{U}_t=\boldsymbol{\Omega}\begin{pmatrix}x_1(t)\\x_2(t)\end{pmatrix}\cdot\boldsymbol{f_k}+\tilde{\boldsymbol{\lambda}}(x_1,x_2,0), \tag{24}$$

where

$$\begin{pmatrix}x_1(t)\\x_2(t)\end{pmatrix}=(\boldsymbol{\Psi},\langle\boldsymbol{U}_t,\boldsymbol{f_k}\rangle).$$

Then, we count the normal form of Eq. (22) on the center manifold. Letting $z=x_1-\mathrm{i}x_2$ and noticing that $\boldsymbol{p}_1=\boldsymbol{\Omega}_1+\mathrm{i}\boldsymbol{\Omega}_2$, Eq. (23) can be rewritten as

$$\boldsymbol{U}_t=\frac{1}{2}(\boldsymbol{p}_1z+\bar{\boldsymbol{p}}_1\bar z)\cdot\boldsymbol{f_k}+\boldsymbol{\Theta}(z,\bar z), \tag{25}$$

where $\boldsymbol{\Theta}(z,\bar z)=\boldsymbol{\lambda}(\frac{z+\bar z}{2},-\frac{z-\bar z}{2\mathrm{i}},0)$. It is easy to get z satisfying

$$\dot z=\mathrm{i}w_0\tau^*z+g(z,\bar z), \tag{26}$$

where

$$\begin{aligned}g(z,\bar z)&=(\boldsymbol{\Psi}_1(0)-\mathrm{i}\boldsymbol{\Psi}_2(0))\langle\boldsymbol{F}(\boldsymbol{U}_t,0),\boldsymbol{f_k}\rangle\\&=(\boldsymbol{\Psi}_1(0)-\mathrm{i}\boldsymbol{\Psi}_2(0))\langle\boldsymbol{f}(\boldsymbol{U}_t,0),\boldsymbol{f_k}\rangle.\end{aligned}$$

Let

$$\boldsymbol{\Theta}(z,\bar z)=\boldsymbol{\Theta}_{20}\frac{z^2}{2}+\boldsymbol{\Theta}_{11}z\bar z+\boldsymbol{\Theta}_{02}\frac{\bar z^2}{2}+\cdots, \tag{27}$$

$$g(z,\bar z)=g_{20}\frac{z^2}{2}+g_{11}z\bar z+g_{02}\frac{\bar z^2}{2}+\cdots. \tag{28}$$

Through Eqs. (25) and (27), we can obtain

$$\begin{aligned}\boldsymbol{U}_{1t}(0)&=\boldsymbol{\Theta}_{20}^{(1)}(0)\frac{z^2}{2}+\boldsymbol{\Theta}_{11}^{(1)}(0)z\bar z+\boldsymbol{\Theta}_{02}^{(1)}(0)\frac{\bar z^2}{2}\\&\quad+\frac{1}{2}(z+\bar z)\cos kx,\\ \boldsymbol{U}_{2t}(0)&=\boldsymbol{\Theta}_{20}^{(2)}(0)\frac{z^2}{2}+\boldsymbol{\Theta}_{11}^{(2)}(0)z\bar z+\boldsymbol{\Theta}_{02}^{(2)}(0)\frac{\bar z^2}{2}\\&\quad+\frac{1}{2}(\xi z+\bar\xi\bar z)\cos kx,\\ \boldsymbol{U}_{1t}(-1)&=\boldsymbol{\Theta}_{20}^{(1)}(-1)\frac{z^2}{2}+\boldsymbol{\Theta}_{11}^{(1)}(-1)z\bar z+\boldsymbol{\Theta}_{02}^{(1)}(-1)\frac{\bar z^2}{2}\\&\quad+\frac{1}{2}(z\mathrm{e}^{-\mathrm{i}w_0\tau^*}+\bar z\mathrm{e}^{\mathrm{i}w_0\tau^*})\cos kx,\\ \boldsymbol{U}_{2t}(-1)&=\boldsymbol{\Theta}_{20}^{(2)}(-1)\frac{z^2}{2}+\boldsymbol{\Theta}_{11}^{(2)}(-1)z\bar z+\boldsymbol{\Theta}_{02}^{(2)}(-1)\frac{\bar z^2}{2}\\&\quad+\frac{1}{2}(\xi z\mathrm{e}^{-\mathrm{i}w_0\tau^*}+\bar\xi\bar z\mathrm{e}^{\mathrm{i}w_0\tau^*})\cos kx.\end{aligned}$$

Combining with Eq. (16), we can get

$$\begin{aligned}f_1(\boldsymbol{U}_t,0)&=\tau^*\cos^2kx\left[\varepsilon_{20}\frac{z^2}{2}+\varepsilon_{11}z\bar z+\varepsilon_{02}\frac{\bar z^2}{2}\right]\\&\quad+\frac{z^2\bar z}{2}[\varepsilon_1\cos kx+\varepsilon_2\cos^3kx]+\cdots,\\ f_2(\boldsymbol{U}_t,0)&=\tau^*\cos^2kx\left[\iota_{20}\frac{z^2}{2}+\iota_{11}z\bar z+\iota_{02}\frac{\bar z^2}{2}\right]\\&\quad+\frac{z^2\bar z}{2}[\iota_1\cos kx+\iota_2\cos^3kx]+\cdots,\\ f_3(\boldsymbol{U}_t,0)&=0,\end{aligned}$$

where the coefficients can be expressed as

$$\begin{aligned}\varepsilon_{20}&=\frac{1}{2}(a_{14}\xi\,\mathrm{e}^{-\mathrm{i}w_0\tau^*}+a_{15}\xi^2\mathrm{e}^{-2\mathrm{i}w_0\tau^*}),\quad \varepsilon_{02}=\bar\varepsilon_{20},\\ \varepsilon_{11}&=\frac{1}{4}a_{14}(\xi\,\mathrm{e}^{-\mathrm{i}w_0\tau^*}+\bar\xi\,\mathrm{e}^{\mathrm{i}w_0\tau^*})+\frac{1}{2}a_{15}\xi\bar\xi,\\ \iota_{20}&=\frac{1}{2}(a_{24}\xi\,\mathrm{e}^{-\mathrm{i}w_0\tau^*}+a_{25}\xi^2\mathrm{e}^{-2\mathrm{i}w_0\tau^*}),\quad \iota_{02}=\bar\iota_{20},\\ \varepsilon_{11}&=\frac{1}{4}a_{24}(\xi\,\mathrm{e}^{-\mathrm{i}w_0\tau^*}+\bar\xi\,\mathrm{e}^{\mathrm{i}w_0\tau^*})+\frac{1}{2}a_{25}\xi\bar\xi,\end{aligned}$$

and

$$\begin{aligned}\varepsilon_1&=a_{14}\left[\boldsymbol{\Theta}_{11}^{(2)}(-1)+\frac{1}{2}\boldsymbol{\Theta}_{20}^{(2)}(-1)+\frac{1}{2}\bar\xi\,\mathrm{e}^{\mathrm{i}w_0\tau^*}\boldsymbol{\Theta}_{20}^{(1)}(0)\right.\\&\quad\left.+\xi\,\mathrm{e}^{-\mathrm{i}w_0\tau^*}\boldsymbol{\Theta}_{11}^{(1)}(0)\right]\\&\quad+a_{15}\left[2\xi\boldsymbol{\Theta}_{11}^{(2)}(-1)\mathrm{e}^{-\mathrm{i}w_0\tau^*}+\bar\xi\boldsymbol{\Theta}_{20}^{(2)}(-1)\mathrm{e}^{\mathrm{i}w_0\tau^*}\right],\\ \varepsilon_2&=\frac{1}{2}a_{16}\xi\bar\xi+\frac{1}{4}a_{16}\xi^2\mathrm{e}^{-2\mathrm{i}w_0\tau^*}+\frac{3}{4}a_{17}\xi^2\bar\xi\,\mathrm{e}^{-\mathrm{i}w_0\tau^*},\\ \iota_1&=a_{24}\left[\boldsymbol{\Theta}_{11}^{(2)}(-1)+\frac{1}{2}\boldsymbol{\Theta}_{20}^{(2)}(-1)+\frac{1}{2}\bar\xi\,\mathrm{e}^{\mathrm{i}w_0\tau^*}\boldsymbol{\Theta}_{20}^{(1)}(0)\right.\\&\quad\left.+\xi\,\mathrm{e}^{-\mathrm{i}w_0\tau^*}\boldsymbol{\Theta}_{11}^{(1)}(0)\right]\\&\quad+a_{25}\left[2\xi\boldsymbol{\Theta}_{11}^{(2)}(-1)\mathrm{e}^{-\mathrm{i}w_0\tau^*}+\bar\xi\boldsymbol{\Theta}_{20}^{(2)}(-1)\mathrm{e}^{\mathrm{i}w_0\tau^*}\right],\\ \iota_2&=\frac{1}{2}a_{26}\xi\bar\xi+\frac{1}{4}a_{26}\xi^2\mathrm{e}^{-2\mathrm{i}w_0\tau^*}+\frac{3}{4}a_{27}\xi^2\bar\xi\,\mathrm{e}^{-\mathrm{i}w_0\tau^*}\\&\quad+\frac{3}{4}k_2\xi^2\bar\xi.\end{aligned}$$

It is noted that

$$\frac{1}{\pi}\int_0^{\pi}\cos^3 kx\mathrm{d}x = 1, \quad k=0,$$
$$\frac{1}{\pi}\int_0^{\pi}\cos^3 kx\mathrm{d}x = 0, \quad k\in\mathbb{N}^+.$$

Let $(\hbar_1,\hbar_2) = \boldsymbol{\Psi}_1(0) - \mathrm{i}\boldsymbol{\Psi}_2(0)$. Considering Eqs. (27) and (28), we have

$$g_{20} = \begin{cases} 0, & k\in\mathbb{N}^+, \\ \tau^*(\varepsilon_{20}\hbar_1 + \iota_{20}\hbar_2), & k=0, \end{cases}$$
$$g_{11} = \begin{cases} 0, & k\in\mathbb{N}^+, \\ \tau^*(\varepsilon_{11}\hbar_1 + \iota_{11}\hbar_2), & k=0, \end{cases}$$
$$g_{02} = \bar{g}_{20},$$
$$g_{21} = \tau^*(\chi_1\hbar_1 + \chi_2\hbar_2), \quad k\in\mathbb{N}.$$

As shown above, we get the expressions of g_{20}, g_{11} and g_{02} when $\theta\in[-1,0]$. In order to get the expression of g_{21}, we must compute $\boldsymbol{\Theta}_{20}(\theta)$ and $\boldsymbol{\Theta}_{11}(\theta)$. From Eq. (27), we know that

$$\dot{\boldsymbol{\Theta}}(z,\bar{z}) = \boldsymbol{\Theta}_{20}z\dot{z} + \boldsymbol{\Theta}_{11}(\dot{z}\bar{z}+\bar{z}\dot{z}) + \boldsymbol{\Theta}_{02}\dot{\bar{z}}\bar{z} + \cdots, \tag{29}$$
$$\boldsymbol{A}_{\tau^*}\boldsymbol{\Theta}(z,\bar{z}) = A_{\tau^*}\boldsymbol{\Theta}_{20}\frac{z^2}{2} + A_{\tau^*}\boldsymbol{\Theta}_{11}z\bar{z} + A_{\tau^*}\boldsymbol{\Theta}_{02}\frac{\bar{z}^2}{2} + \cdots. \tag{30}$$

Otherwise, $\boldsymbol{\Theta}(z(t),\bar{z}(t))$ satisfies

$$\dot{\boldsymbol{\Theta}} = \boldsymbol{A}_{\tau^*}\boldsymbol{\Theta} + \boldsymbol{\Pi}(z,\bar{z}), \tag{31}$$

where

$$\begin{aligned}\boldsymbol{\Pi}(z,\bar{z}) &= \boldsymbol{\Pi}_{20}\frac{z^2}{2} + \boldsymbol{\Pi}_{11}z\bar{z} + \boldsymbol{\Pi}_{02}\frac{\bar{z}^2}{2} + \cdots \\ &= \boldsymbol{X}_0\boldsymbol{F}(\boldsymbol{U}_t{}^*,0) - \boldsymbol{\Omega}(\boldsymbol{\Psi},\langle\boldsymbol{X}_0\boldsymbol{F}(\boldsymbol{U}_t{}^*,0),\boldsymbol{f}_k\rangle)\cdot\boldsymbol{f}_k \\ &= \boldsymbol{X}_0\boldsymbol{f}(\boldsymbol{U}_t{}^*,0) - \boldsymbol{\Omega}(\boldsymbol{\Psi},\langle\boldsymbol{X}_0\boldsymbol{f}(\boldsymbol{U}_t{}^*,0),\boldsymbol{f}_k\rangle)\cdot\boldsymbol{f}_k. \end{aligned}\tag{32}$$

Comparing the coefficients in Eq. (29) with those in Eq. (31), it follows that

$$\begin{cases} (2\mathrm{i}w_0\tau^* - \boldsymbol{A}_{\tau^*})\boldsymbol{\Theta}_{20}(\theta) = \boldsymbol{\Pi}_{20}(\theta), \\ -\boldsymbol{A}_{\tau^*}\boldsymbol{\Theta}_{11}(\theta) = \boldsymbol{\Pi}_{11}(\theta). \end{cases} \tag{33}$$

By Eq. (32), we can see that

$$\begin{aligned}\boldsymbol{\Pi}(z,\bar{z}) &= -\boldsymbol{\Omega}(\theta)\boldsymbol{\Psi}(0)\langle\boldsymbol{X}_0\boldsymbol{F}(\boldsymbol{U}_t,0),\boldsymbol{f}_k\rangle\cdot\boldsymbol{f}_k \\ &= -\left(\frac{\boldsymbol{p}_1(\theta)+\boldsymbol{p}_2(\theta)}{2}, \frac{\boldsymbol{p}_1(\theta)-\boldsymbol{p}_2(\theta)}{2\mathrm{i}}\right) \\ &\quad\times(\boldsymbol{\Psi}_1(0),\boldsymbol{\Psi}_2(0))^{\mathrm{T}}\times\langle\boldsymbol{f}(\boldsymbol{U}_t,0),\boldsymbol{f}_k\rangle\cdot\boldsymbol{f}_k \\ &= -\frac{1}{4}[g_{20}\boldsymbol{p}_1(\theta)+\bar{g}_{02}\boldsymbol{p}_2(\theta)]z^2\cdot\boldsymbol{f}_k \\ &\quad -\frac{1}{2}[g_{11}\boldsymbol{p}_1(\theta)+\bar{g}_{11}\boldsymbol{p}_2(\theta)]z\bar{z}\cdot\boldsymbol{f}_k + \cdots. \end{aligned}$$

When $\theta\in[-1,0)$,

$$\boldsymbol{\Pi}_{20}(\theta) = \begin{cases} 0, & k=\mathbb{N}^+, \\ -\frac{1}{2}[g_{20}\boldsymbol{p}_1(\theta)+\bar{g}_{02}\boldsymbol{p}_2(\theta)]\cdot\boldsymbol{f}_0, & k=0, \end{cases}$$
$$\boldsymbol{\Pi}_{11}(\theta) = \begin{cases} 0, & k=\mathbb{N}^+, \\ -\frac{1}{2}[g_{11}\boldsymbol{p}_1(\theta)+\bar{g}_{11}\boldsymbol{p}_2(\theta)]\cdot\boldsymbol{f}_0, & k=0. \end{cases}$$

When $k=0$,

$$\begin{aligned}&\boldsymbol{\Pi}_{20}(0) \\ &= \begin{cases} \tau^*\begin{pmatrix}\varepsilon_{20}\\ \iota_{20}\\ 0\end{pmatrix}\cos^2 kx, & k=\mathbb{N}^+, \\ \tau^*\begin{pmatrix}\varepsilon_{20}\\ \iota_{20}\\ 0\end{pmatrix} - \frac{1}{2}[g_{20}\boldsymbol{p}_1(0)+\bar{g}_{02}\boldsymbol{p}_2(0)]\cdot\boldsymbol{f}_0, & k=0, \end{cases} \\ &\boldsymbol{\Pi}_{11}(0) \\ &= \begin{cases} \tau^*\begin{pmatrix}\varepsilon_{11}\\ \iota_{11}\\ 0\end{pmatrix}\cos^2 kx, & k=\mathbb{N}^+, \\ \tau^*\begin{pmatrix}\varepsilon_{11}\\ \iota_{11}\\ 0\end{pmatrix} - \frac{1}{2}[g_{11}\boldsymbol{p}_1(0)+\bar{g}_{11}\boldsymbol{p}_2(0)]\cdot\boldsymbol{f}_0, & k=0. \end{cases}\end{aligned}$$

By the definition of $\boldsymbol{A}_{\tau^*}$, when $\theta\in[-1,0)$, we can get

$$\dot{\boldsymbol{\Theta}}_{20}(\theta) = \begin{cases} 2\mathrm{i}w_0\tau^*\boldsymbol{\Theta}_{20}(\theta), & k\in\mathbb{N}^+, \\ 2\mathrm{i}w_0\tau^*\boldsymbol{\Theta}_{20}(\theta) + \frac{1}{2}[g_{20}\boldsymbol{p}_1(\theta)+\bar{g}_{02}\boldsymbol{p}_2(\theta)]\cdot\boldsymbol{f}_k, & k=0. \end{cases}$$

Furthermore, since $\boldsymbol{p}(\theta) = \boldsymbol{p}(0)\mathrm{e}^{\mathrm{i}w_0\tau^*\theta}$, it follows that

$$\boldsymbol{\Theta}_{20}(\theta) = \begin{cases} \boldsymbol{E}_1\mathrm{e}^{2\mathrm{i}w_0\tau^*\theta}, & k\in\mathbb{N}^+, \\ \frac{1}{2}\left[\frac{\mathrm{i}g_{20}}{w_0\tau^*}\boldsymbol{p}_1(\theta) + \frac{\mathrm{i}\bar{g}_{02}}{3w_0\tau^*}\boldsymbol{p}_2(\theta)\right]\cdot\boldsymbol{f}_0 + \boldsymbol{E}_1\mathrm{e}^{2\mathrm{i}w_0\tau^*\theta}, & k=0, \end{cases} \tag{34}$$

with

$$\boldsymbol{E}_1 = \begin{cases} \boldsymbol{\Theta}_{20}(0), & k\in\mathbb{N}^+, \\ \boldsymbol{\Theta}_{20}(0) - \frac{1}{2}\left[\frac{\mathrm{i}g_{20}}{w_0\tau^*}\boldsymbol{p}_1(0) + \frac{\mathrm{i}\bar{g}_{02}}{3w_0\tau^*}\boldsymbol{p}_2(0)\right]\cdot\boldsymbol{f}_0, & k=0. \end{cases} \tag{35}$$

Using the definition of $\boldsymbol{A}_{\tau^*}$ and combining Eqs. (33)–(35), for $k\in\mathbb{N}^+$, we get

$$
\begin{aligned}
&2\mathrm{i}w_0\tau^*\Theta_{20}(0)-\tau^*\boldsymbol{D}\Delta\Theta_{20}(0)-\boldsymbol{L}(\tau^*)(\Theta_{20}(\theta))\\
=\;&2\mathrm{i}w_0\tau^*\boldsymbol{E}_1-\tau^*\boldsymbol{D}\Delta\boldsymbol{E}_1-\boldsymbol{L}(\tau^*)(\boldsymbol{E}_1\mathrm{e}^{2\mathrm{i}w_0\tau^*\theta})\\
=\;&\tau^*\begin{pmatrix}\varepsilon_{20}\\ \iota_{20}\\ 0\end{pmatrix}\cos^2 kx.
\end{aligned}
$$

Hence,

$$
\boldsymbol{E}_1=\begin{pmatrix}\kappa_1 & 0 & 0\\ -a_{21} & \kappa_2 & 0\\ -a_{31} & -b_{32}\mathrm{e}^{-2\mathrm{i}w_0\tau^*} & \kappa_3\end{pmatrix}^{-1}\begin{pmatrix}\varepsilon_{20}\\ \iota_{20}\\ 0\end{pmatrix}\cos^2 kx, \quad (36)
$$

where

$$
\begin{aligned}
&\kappa_1=2\mathrm{i}w_0+d_1k^2-a_{11},\\
&\kappa_2=2\mathrm{i}w_0+d_2'k^2-a_{22}-b_{22}\mathrm{e}^{-2\mathrm{i}w_0\tau^*},\\
&\kappa_3=2\mathrm{i}w_0+d_3k^2-a_{33}.
\end{aligned}
$$

When $k=0$, we have

$$
\begin{aligned}
&2\mathrm{i}w_0\tau^*\Theta_{20}(0)-\tau^*\boldsymbol{D}\Delta\,\Theta_{20}(0)-\boldsymbol{L}(\tau^*)\Theta_{20}(\theta)\\
=\;&2\mathrm{i}w_0\tau^*\left[\frac{1}{2}\left[\frac{\mathrm{i}g_{20}}{w_0\tau^*}\boldsymbol{p}_1(0)+\frac{\mathrm{i}\bar{g}_{02}}{3w_0\tau^*}\boldsymbol{p}_2(0)\right]\cdot\boldsymbol{f}_0+\boldsymbol{E}_1\right]\\
&-\tau^*\boldsymbol{D}\Delta\left[\frac{1}{2}\left[\frac{\mathrm{i}g_{20}}{w_0\tau^*}\boldsymbol{p}_1(0)+\frac{\mathrm{i}\bar{g}_{02}}{3w_0\tau^*}\boldsymbol{p}_2(0)\right]\cdot\boldsymbol{f}_0+\boldsymbol{E}_1\right]\\
&-\boldsymbol{L}(\tau^*)\left[\frac{1}{2}\left[\frac{\mathrm{i}g_{20}}{w_0\tau^*}\boldsymbol{p}_1(0)+\frac{\mathrm{i}\bar{g}_{02}}{3w_0\tau^*}\boldsymbol{p}_2(0)\right]\cdot\boldsymbol{f}_0\right.\\
&\left.+\boldsymbol{E}_1\mathrm{e}^{2\mathrm{i}w_0\tau^*\theta}\right]\\
=\;&\tau^*\begin{pmatrix}\varepsilon_{20}\\ \iota_{20}\\ 0\end{pmatrix}-\frac{1}{2}[\boldsymbol{p}_1(0)g_{20}+\boldsymbol{p}_2(0)g_{02}]\cdot\boldsymbol{f}_0.
\end{aligned}
$$

In addition, due to

$$
\begin{cases}\tau^*\boldsymbol{D}\Delta[\boldsymbol{p}_1(0)\cdot\boldsymbol{f}_0]+\boldsymbol{L}(\tau^*)[\boldsymbol{p}_1(\theta)\cdot\boldsymbol{f}_0]=\mathrm{i}w_0\tau^*\boldsymbol{p}_1(0)\cdot\boldsymbol{f}_0,\\ \tau^*\boldsymbol{D}\Delta[\boldsymbol{p}_2(0)\cdot\boldsymbol{f}_0]+\boldsymbol{L}(\tau^*)[\boldsymbol{p}_2(\theta)\cdot\boldsymbol{f}_0]=-\mathrm{i}w_0\tau^*\boldsymbol{p}_2(0)\cdot\boldsymbol{f}_0,\end{cases}
$$

we obtain

$$
2\mathrm{i}w_0\tau^*\boldsymbol{E}_1-\tau^*\boldsymbol{D}\Delta\boldsymbol{E}_1-\boldsymbol{L}(\tau^*)(\boldsymbol{E}_1\mathrm{e}^{2\mathrm{i}w_0\tau^*\theta})=\tau^*\begin{pmatrix}\varepsilon_{20}\\ \iota_{20}\\ 0\end{pmatrix}.
$$

Thus, when $k=0$,

$$
\boldsymbol{E}_1=\begin{pmatrix}\kappa_1 & -b_{12}\mathrm{e}^{-2\mathrm{i}w_0\tau^*} & 0\\ -a_{21} & \kappa_2 & 0\\ -a_{31} & -b_{32}\mathrm{e}^{-2\mathrm{i}w_0\tau^*} & \kappa_3\end{pmatrix}^{-1}\times\begin{pmatrix}\varepsilon_{20}\\ \iota_{20}\\ 0\end{pmatrix}\cos^2 kx, \quad (37)
$$

where

$$
\begin{aligned}
&\sigma_1=2\mathrm{i}w_0-a_{11},\\
&\sigma_2=2\mathrm{i}w_0-a_{22}-b_{22}\mathrm{e}^{-2\mathrm{i}w_0\tau^*},\\
&\sigma_3=2\mathrm{i}w_0-a_{33}.
\end{aligned}
$$

Finally, from Eqs. (36) and (37), $\forall k\in\mathbb{N}$, it is easy to get

$$
\boldsymbol{E}_1=\begin{pmatrix}\kappa_1 & -b_{12}\mathrm{e}^{-2\mathrm{i}w_0\tau^*} & 0\\ -a_{21} & \kappa_2 & 0\\ -a_{31} & -b_{32}\mathrm{e}^{-2\mathrm{i}w_0\tau^*} & \kappa_3\end{pmatrix}^{-1}\times\begin{pmatrix}\varepsilon_{20}\\ \iota_{20}\\ 0\end{pmatrix}\cos^2 kx.
$$

Using the calculations in Eqs. (34)–(37), we get

$$
\dot{\Theta}_{11}(\theta)=\begin{cases}0, & k\in\mathbb{N}^+,\\ \dfrac{1}{2}[g_{11}\boldsymbol{p}_1(\theta)+\bar{g}_{11}\boldsymbol{p}_2(\theta)]\cdot\boldsymbol{f}_0, & k=0,\end{cases}
$$

$$
\Theta_{11}(\theta)=\begin{cases}\boldsymbol{E}_2, & k\in\mathbb{N}^+,\\ \dfrac{1}{2}\left[\dfrac{-\mathrm{i}g_{11}}{w_n\tau^*}\boldsymbol{p}_1(\theta)+\dfrac{\mathrm{i}\bar{g}_{11}}{w_n\tau^*}\boldsymbol{p}_2(\theta)\right]\cdot\boldsymbol{f}_0+\boldsymbol{E}_2, & k=0,\end{cases}
$$

where

$$
\begin{aligned}
\boldsymbol{E}_2=\;&\begin{pmatrix}e_1 & -b_{12} & 0\\ -a_{21} & e_2 & 0\\ -a_{31} & -b_{32} & e_3\end{pmatrix}^{-1}\\
&\times\begin{pmatrix}\varepsilon_{11}\\ \iota_{11}\\ 0\end{pmatrix}\cos^2 kx, \quad k\in\mathbb{N}, \qquad (38)
\end{aligned}
$$

with

$$
\begin{aligned}
&e_1=d_1k^2-a_{11},\\
&e_2=d_2'k^2-a_{22}-b_{22},\\
&e_3=d_3k^2-a_{33}.
\end{aligned}
$$

Summarizing the previous results, we can get a specific expression for g_{21}. To determine the Hopf bifurcation direction, the stability and period of system (3) at the critical value τ^*, we give the following formula:

$$
\begin{aligned}
&c_1(0)=\frac{\mathrm{i}}{2w_0\tau^*}\left(g_{20}g_{11}-2|g_{11}|^2-\frac{|g_{02}|^2}{3}\right)+\frac{g_{21}}{2},\\
&\mu_2=-\frac{\mathrm{Re}(c_1(0))}{\mathrm{Re}(\lambda'(\tau^*))},\\
&\beta_2=2\mathrm{Re}(c_1(0)),\\
&T_2=-\frac{\mathrm{Im}(c_1(0))+\mu_2\mathrm{Im}(\lambda'(\tau^*))}{w_0\tau^*}.
\end{aligned}
$$

We can obtain the following theorem.

Theorem 3 For the Hopf bifurcation generated by system (3) at any critical value τ^* , we have

1. The direction of the Hopf bifurcation is determined by μ_2. If $\mu_2<0$ ($\mu_2>0$), then the Hopf bifurcation direction is subcritical (supercritical).

2. β_2 determines the stability of bifurcating periodic. If $\beta_2<0$ ($\beta_2>0$), then the periodic solutions are stable (unstable).

3. The period of the bifurcating periodic solutions is determined by T_2. If $T_2<0$ ($T_2>0$), then the period decreases (increases).

5. Numerical simulations

This section uses MATLAB software to simulate and verify the theoretical results from the previous analysis. We select the appropriate system parameters

$$
A=0.04,\quad b=-0.1,\quad \beta=1.4,
$$

$$\mu_1 = 0.04, \quad \sigma = 0.02, \quad \gamma = 0.08.$$

By calculating, we get the basic reproduction number $R_0 = 7.78$ and the positive equilibrium point $E_1 = (0.0832,\ 0.2917,\ 0.6251)$. At this time, (H_1) holds.

5.1. Analysis of Turing instability and control

We choose the initial conditions as follows:

$$S(x,0) = 0.0832 + 0.1\cos x,$$
$$I(x,0) = 0.2917 + 0.1\cos x,$$
$$R(x,0) = 0.6251 + 0.1\cos x.$$

In the following, we discuss the different values of the diffusion coefficient and controller parameters separately.

Case 1: $\tau = 0,\ d_1 = d_2 = d_3 = 0.$

According to Theorem 1, it is easy to get the uncontrolled system (2) is locally asymptotically stable at E_1. As can be seen from Fig. 1, the spatial profiles of the state nodes eventually converge to the equilibrium point, which is consistent with the theoretical results.

Case 2: $\tau = 0,\ d_1 = 2,\ d_2 = 0.001,\ d_3 = 0.001.$

Under this set of parameters, (H_2) and (H_3) are satisfied. As can be seen from Fig. 2, Turing instability occurs and system (2) is unstable under the action of diffusion term. At the same time, from Fig. 3, we note that the spatial graph of the uncontrolled system (2) shows a large oscillation, at which an unstable Turing pattern is generated.

Case 3: $\tau = 0, d_1 = 2, d_2 = 0.001, d_3 = 0.001, k_1 = 1.1,$ $k_2 = -0.009$. We choose the control parameters $k_1 = 1.1$, $k_2 = -0.009$ and (H_4) and (H_5) hold. With the effect of a hybrid controller, the controlled system (3) returns to the steady state as shown in Fig. 4, which indicates that the hybrid control may suppress Turing instability.

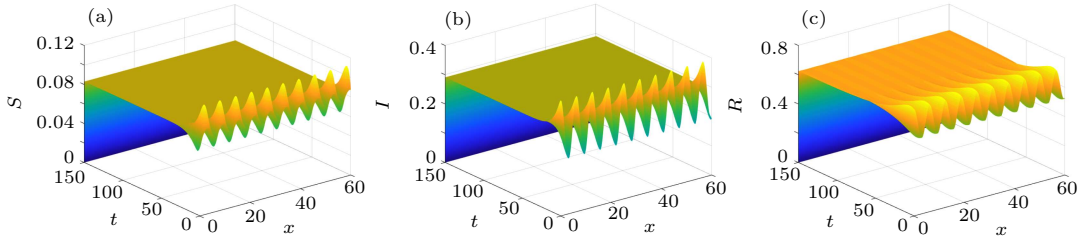


Fig. 1. When $\tau = 0, d_1 = d_2 = d_3 = 0$, the uncontrolled system (2) is locally asymptotically stable at E_1.

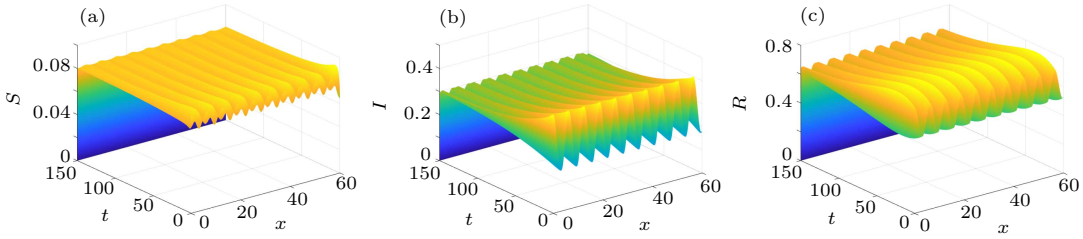


Fig. 2. When $\tau = 0, d_1 = 2, d_2 = 0.001, d_3 = 0.001$, Turing instability occurs in the uncontrolled system (2).

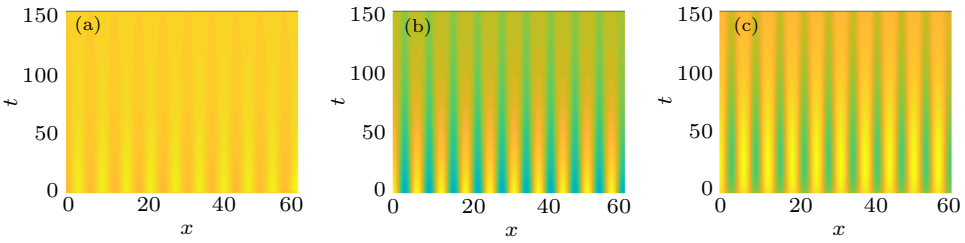


Fig. 3. Turing pattern of system (2) when Turing instability occurs.

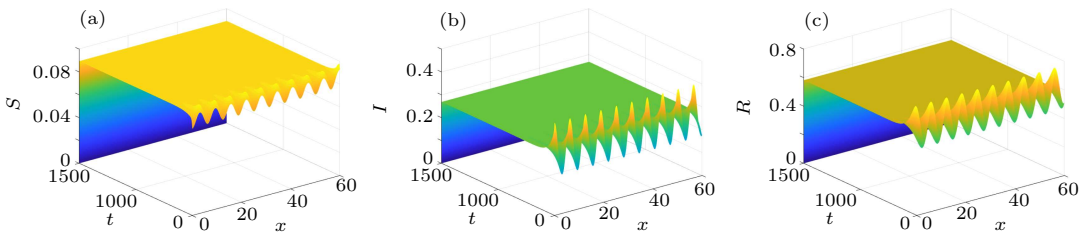


Fig. 4. When $k_1 = 1.1, k_2 = -0.009$, the controlled system (3) returns to the stable state.

5.2. Analysis of Hopf bifurcation and control

Next, we keep the parameters of system (2) as in the above. Let $d_1 = 2$, $d_2 = 0.001$, $d_3 = 0.001$, and choose $S(x,0) = 0.0832$, $I(x,0) = 0.2917$, $R(x,0) = 0.6251$ as initial values. It is clear that (H_1) and (H_6)–(H_{11}) are true. By calculating, we know that $\tau_0 = 40.95$, $w_0 = 0.05$, $\mu_2 = 155.9$, $\beta_2 = -8.9073$, $T_2 = 13.68$.

Case I: Without control

When $\tau = 35 < \tau_0 = 40.95$, according to Theorem 2, system (2) is asymptotically stable at the positive equilibrium point E_1, as shown in Fig. 5. The trajectory of each state node converges to a straight line. From Fig. 6 we can see that system (2) undergoes a Hopf bifurcation and produces a limit cycle at E_1 when $\tau = 42 > \tau_0 = 40.95$.

Case II: Proportional gain control with $k_1 > 0$, $k_2 = 0$.

In contrast to the system (2) displayed in Fig. 6, the controlled system (3) eventually converges to a steady state when $k_1 = 0.5$ and $k_2 = 0$ as displayed in Fig. 7. The stability interval expands and the Hopf bifurcation is delayed, where the bifurcation threshold τ_0 is 63.28. By increasing k_1 to 1.1, the stability interval of the system shrinks, and the Hopf bifurcation occurs early for the controlled system (3) when τ crosses $\tau_0 = 36.97$.

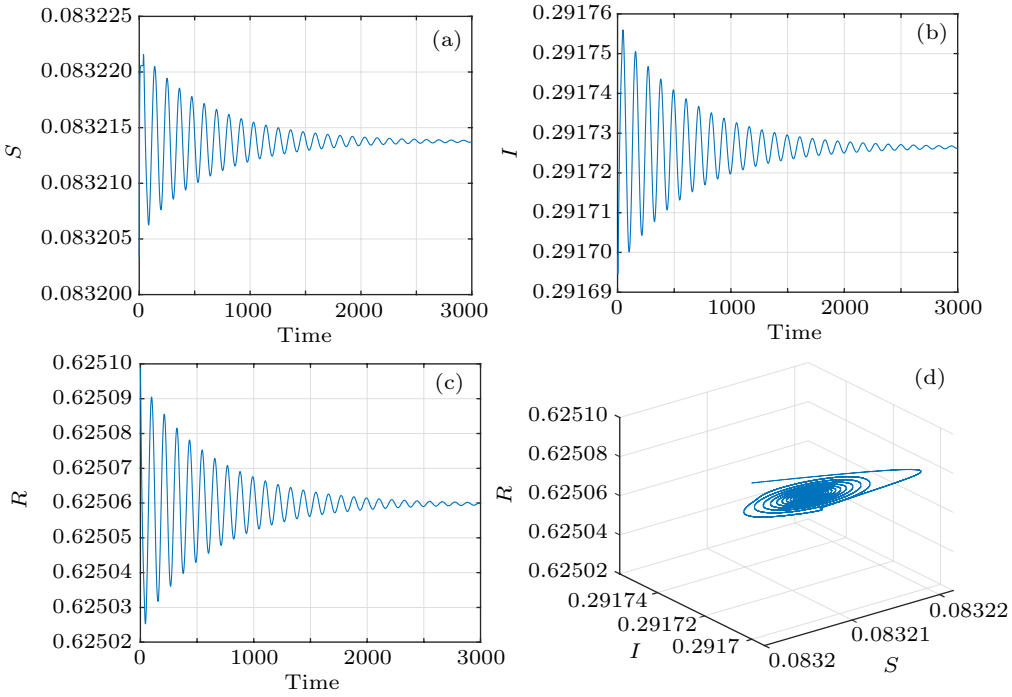


Fig. 5. The waveforms of system (2) for $\tau = 35 < \tau_0 = 40.95$.

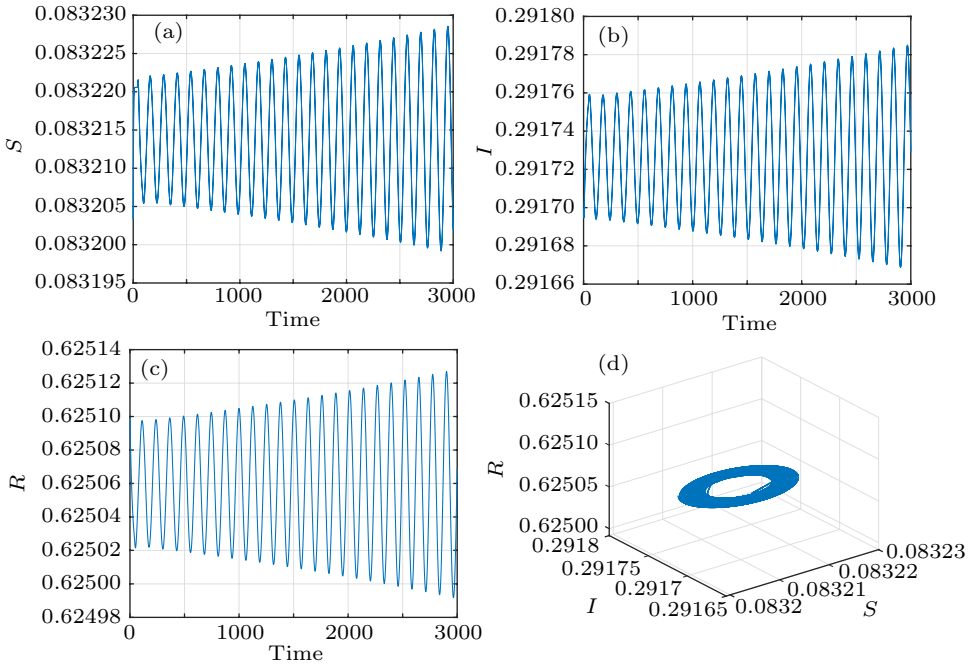


Fig. 6. The waveforms of system (2) for $\tau = 42 > \tau_0 = 40.95$.

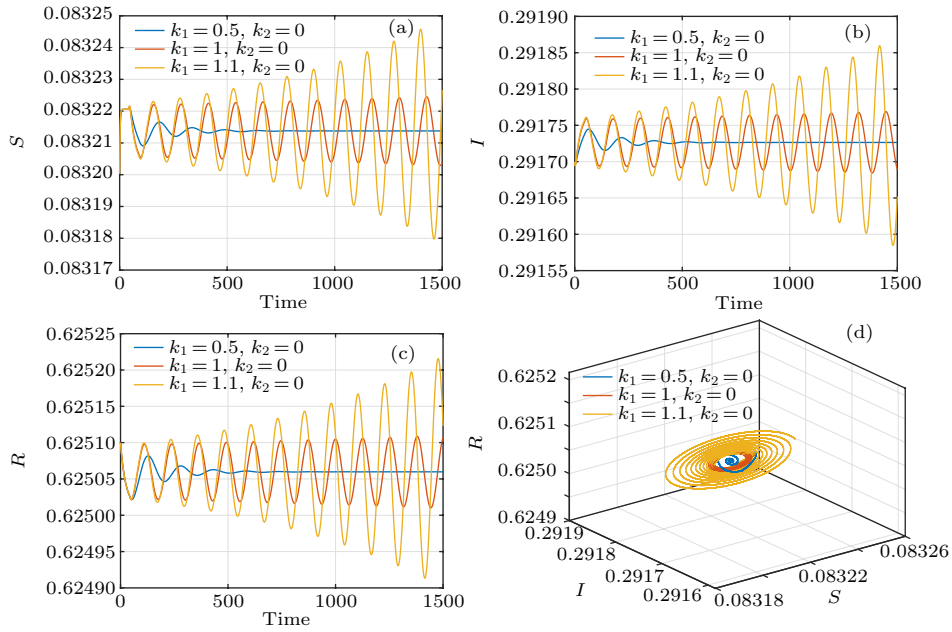


Fig. 7. The waveforms of the controlled system (3) with $\tau = 42$, $k_2 = 0$, and different values of k_1: k_1, respectively, equals 0.5, 1, and 1.1.

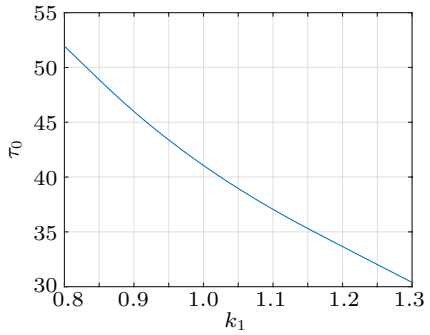


Fig. 8. A graph of the variation of τ_0 with k_1.

By further study, we can see from Fig. 8 that the bifurcation threshold τ_0 varies with k_1. When $k_1 > 1$, the bifurcation threshold of the controlled system (3) is smaller than that of the uncontrolled system (2), triggering Hopf bifurcation in advance. When $0 < k_1 < 1$, the bifurcation threshold of the controlled system (3) is greater than system (2), and the Hopf bifurcation is delayed. Therefore, we can regulate the bifurcation threshold by adjusting the value of k_1.

Case III: State feedback control with $k_1 = 1, -0.02 < k_2 < 0.1$.

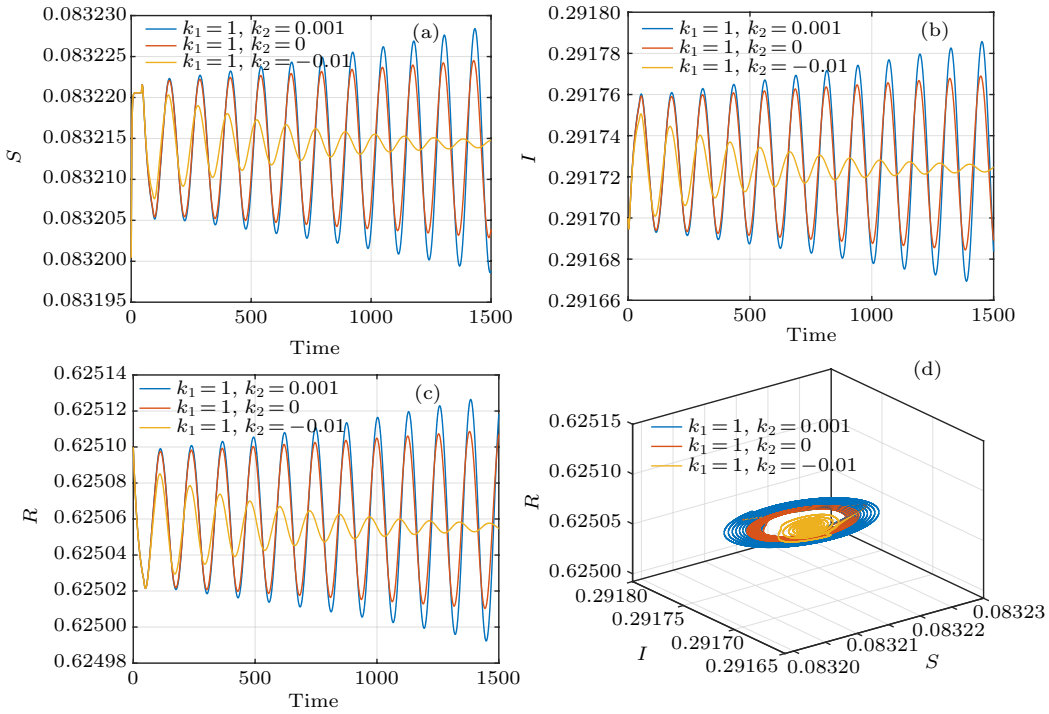


Fig. 9. The waveforms of the controlled system (3) with $\tau = 42$, $k_1 = 1$, and different values of k_2: k_2, respectively, equals -0.01, 0, and 0.001.

In Fig. 9, under the action of the state feedback controller with $k_1 = 1$ and $k_2 = -0.01$, the controlled system (3) eventually converges to a steady state, the stability interval expands, and the Hopf bifurcation is delayed, where $\tau_0 = 56.99$. When $k_1 = 1$ and $k_2 = 0.001$, the Hopf bifurcation of system (3) occurs in advance, while the amplitude of the periodic oscillation gets bigger, where $\tau_0 = 39.90$. It can be seen that the feedback gain parameter k_2 not only affects the location of the bifurcation point but also has a great impact on the amplitude of oscillations. Figure 10 gives the relationship curve between τ_0 and k_2. When $-0.02 < k_2 < -0.001$, the bifurcation threshold of the controlled system (3) is greater than that of system (2), and the Hopf bifurcation is delayed. When $-0.001 < k_2 < 0.1$, the bifurcation threshold of the controlled system (3) is smaller than that of system (2), and the Hopf bifurcation occurs early.

Case IV: Hybrid control with $k_1 \neq 1$, $k_2 \neq 0$.

It is obvious form Fig. 7 that when $k_1 = 1.1$ and $k_2 = 0$, the controlled system (3) undergoes a Hopf bifurcation under the action of k_1. However, when k_2 is reduced to -0.02, the Hopf bifurcation is delayed and the controlled system (3) reverts to the steady state, as shown in Fig. 11. Furthermore, we take $k_1 = 1.1$, $k_2 = 0.002$ and $k_1 = 1.1$, $k_2 = -0.004$. Under these two sets of control gain parameters, we can calculate $\mu_2 = 153.4$, $\beta_2 = -7.1735$, $T_2 = 15.98$ and $\mu_2 = 150.8$, $\beta_2 = -5.0586$, $T_2 = 20.49$, respectively. According to Theorem 3, the controlled system (3) produces a supercritical Hopf bifurcation, possesses a stable bifurcated period solution, and the bifurcating period is increasing. From Fig. 12, we can find that the amplitude of oscillations changes significantly when different values of k_2 are chosen. Thus, it can be concluded that the gain parameter k_2 has an important influence on the nature of Hopf bifurcation.

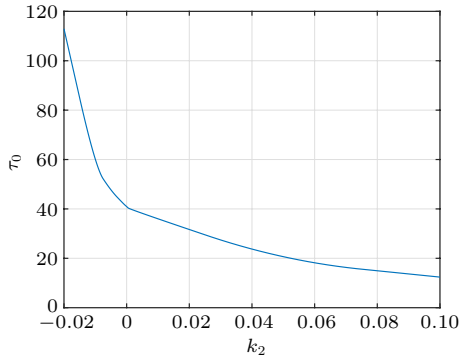


Fig. 10. A graph of the variation of τ_0 with k_2.

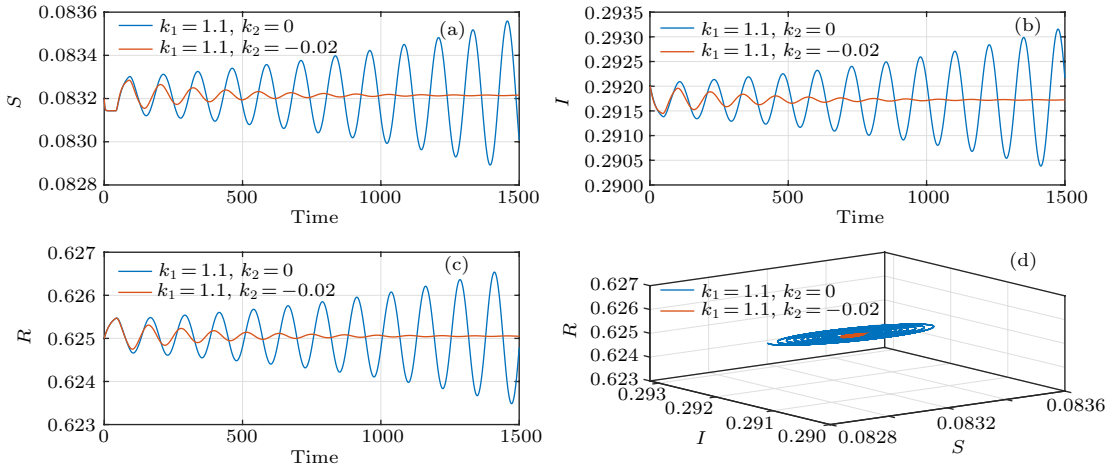


Fig. 11. The waveforms of the controlled system (3) with $\tau = 42$, $k_1 = 1.1$, and different values of k_2: k_2, respectively, equals 0 and -0.02.

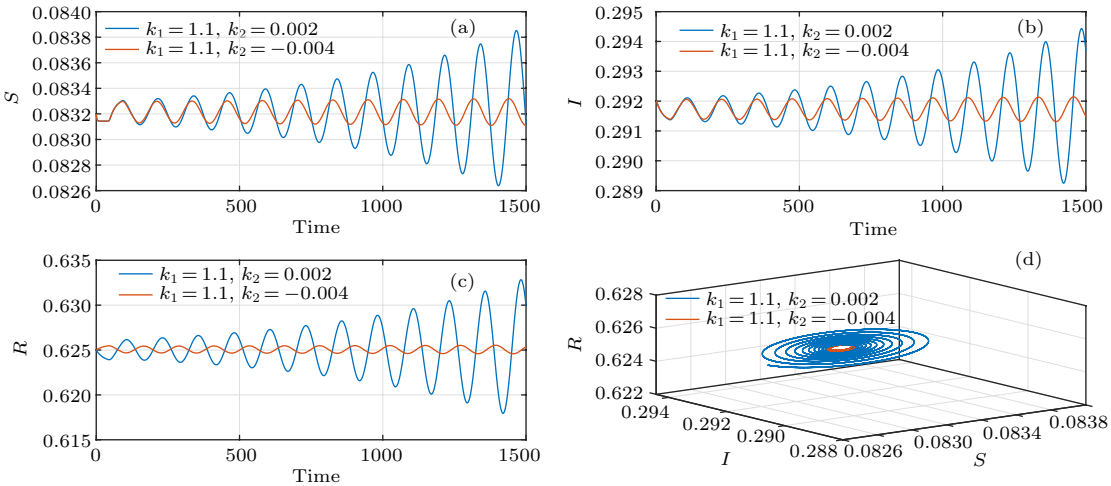


Fig. 12. The waveforms of the controlled system (3) with $\tau = 42$, $k_1 = 1.1$, and different values of k_2: k_2, respectively, equals 0.002 and -0.004.

6. Conclusion

A malware propagation model in MWSNs under hybrid control is established in this paper. Through theoretical analysis and numerical simulations, we can find that diffusion terms will cause Turing instability, and time delay will result in Hopf bifurcation. The conditions for the occurrence of Turing instability and Hopf bifurcation are obtained and the direction of Hopf bifurcation is determined by using the bifurcation theory and the central manifold theorem. The MATLAB simulation results prove that the hybrid control method adopted in this paper can effectively suppress the Turing instability and control the occurrence of Hopf bifurcation. This helps to enhance the stability and controllability of the system to obtain the expected dynamic behavior and reduce potential risks.

The spatial mobility of wireless sensors aggravates the difficulty of preventing and controlling malware propagation. In addition, antivirus software does not act continuously but updates the virus database periodically. Therefore, it is still difficult to design the corresponding optimal controllers for MWSNs. In our future work, we will explore the effects of other control methods in control theory on the system in order to find the optimal control strategy.

Acknowledgements

Project supported by the National Natural Science Foundation of China (Grant No. 62073172) and the Natural Science Foundation of Jiangsu Province of China (Grant No. BK20221329).

References

[1] Wang Y Q and Yang X Y 2013 *Chin. Phys. B* **22** 010509
[2] Wang Y Q and Yang X Y 2013 *Chin. Phys. B* **22** 040206
[3] Li Y and Liu Y 2005 *Chin. Phys. B* **14** 2153
[4] Li Q, Zhang B H and Cui L G 2012 *Chin. Phys. B* **21** 050205
[5] Feng X, Liu L and Zhang F 2022 *Acta Math. Appl. Sin.* **38** 282
[6] Lu Y L, Jiang G P and Song Y R 2012 *Chin. Phys. B* **21** 100207
[7] Ren J, Yang X and Zhu Q 2012 *Nonlinear Anal. Real World Appl.* **13** 376
[8] Chong Y, Kashyap A J and Chen S 2023 *Axioms* **12** 1031
[9] Abdelouahab M S, Arama A and Lozi R 2021 *Chaos* **31** 123125
[10] Zhang Z and Bi D 2016 *Discrete Dyn. Nat. Soc.* **2016** 3067872
[11] ao Y, Fu Q, Yang W, Wang Y and Sheng C 2018 *Secur. Commun. Netw.* **2018** 9756982
[12] Du Y, Niu B and Wei J 2022 *Acta Math. Appl. Sin.* **38** 128
[13] Kumari S and Upadhyay R K 2021 *Math. Comput. Simul.* **190** 246
[14] Yu S, Yu Z and Jiang H 2021 *Inf. Sci.* **581** 18
[15] Lu L, Huang C and Song X 2023 *Eur. Phys. J. Plus* **138** 77
[16] Khan A Q, Bukhari S A H and Almatrafi M B 2022 *Alex. Eng. J.* **61** 11391
[17] Zhu L, Zhao H and Wang X 2015 *Commun. Nonlinear Sci. Numer. Simul.* **22** 747
[18] Mao Z S, Wang H, Xu D D and Cui Z J 2013 *Math. Probl. Eng.* **2013** 315367
[19] Zhou W G 2018 *Physica A* **515** 183
[20] Feng L P, Song L P, Zhao Q S and Wang H B 2015 *Math. Probl. Eng.* **2015** 129598
[21] Zhang Z Z, Chu Y G, H U, Kumari S and Ranjit K U 2019 *Zhejiang Da Xue Xue Bao Li Xue Ban* **46** 172
[22] Wang X M, He Z B, Zhao X Q, Lin C, Pan Y and Cai Z P 2013 *Sci. China Inf. Sci.* **56** 092303
[23] Ding L, Hu P and Guan Z H 2020 *IEEE Trans. Syst. Man Cybern. Syst.* **51** 6779
[24] Ding D W, Zhang X Y, Wang N and Liang D 2017 *J. Shanghai Jiaotong Univ. Sci.* **22** 206
[25] Wu Z, Cai Y and Wang Z 2023 *J. Differ. Equ.* **352** 221
[26] Yang R 2022 *Chaos Solitons Fractals* **164** 112659
[27] Wang S, Ding Y and Lu H 2021 *Math. Biosci. Eng* **18** 5505
[28] Golubitsky M and Langford W F 1981 *J. Differ. Equ.* **41** 375
[29] Gbber F and Willamowski K D 1979 *J. Math. Anal. Appl.* **71** 333
[30] Peng M and Zhang Z 2020 *J. Vib. Control* **26** 1232
[31] Gao Q 2009 *International Workshop on Chaos-Fractals Theories and Applications*, November 6–8, 2009, Shenyang, China, p. 272
[32] Honghua B, Daifeng D and Junjie W 2023 *Math. Biosci. Eng.* **20** 12194
[33] Liu J and Zhang Z 2019 *Adv. Differ. Equ.* **2019** 442
[34] Hsu L and Favretto L 1984 *J. Math. Anal. Appl.* **101** 562
[35] Zeng X, Xiong Z and Wang C 2016 *Appl. Math. Comput.* **282** 17
[36] Chen Y Y and Bi Y Q 2014 *J. Appl. Math.* **2014** 804204
[37] Song L Y, He Y N and Ge Z H 2007 *Appl. Math. Comput.* **190** 677